SCALE-TIME THEORY

THE GEOMETRY OF SCALE-SPACE

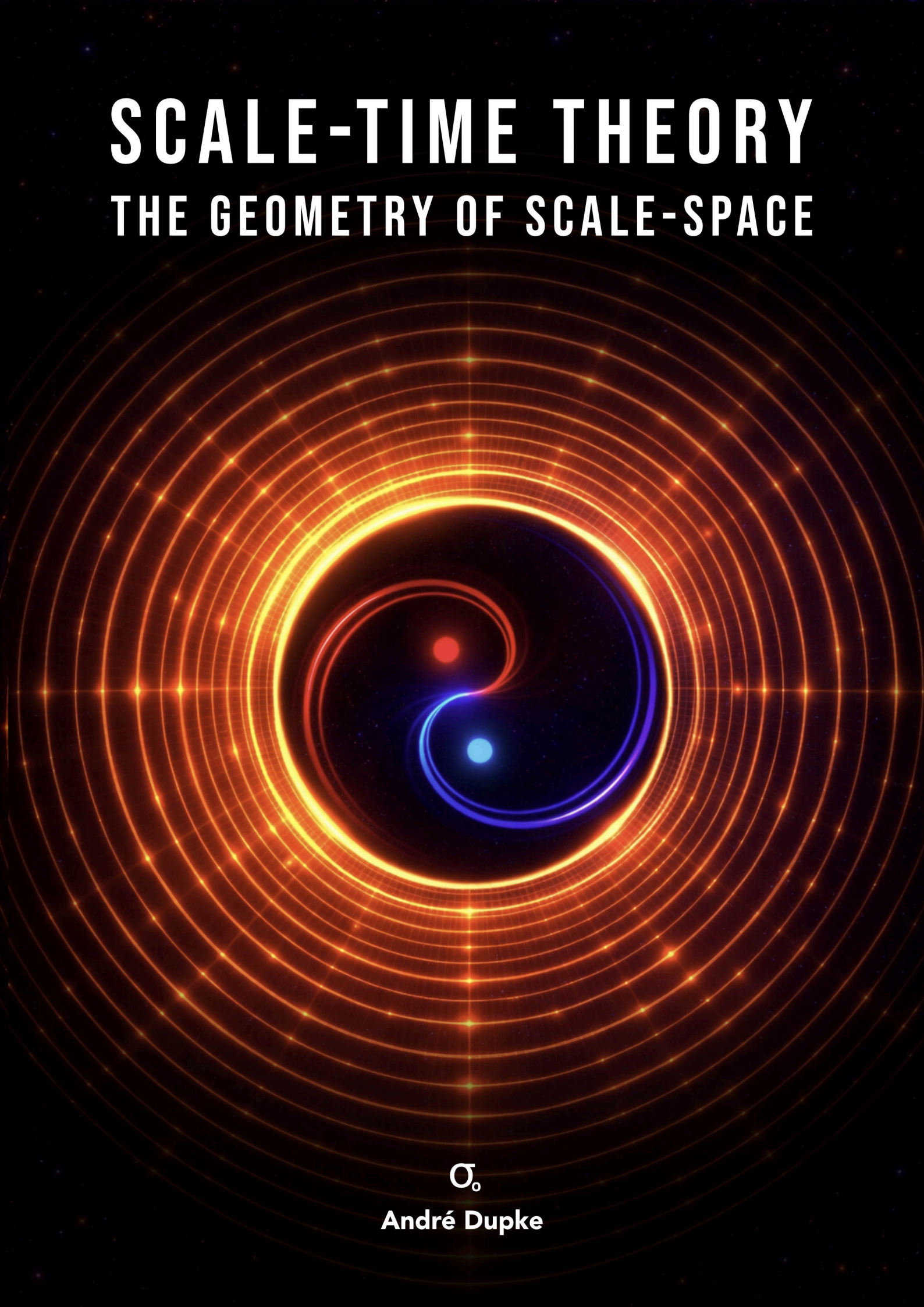

σ_o

André Dupke

Scale-Time Dynamics Research

André Dupke
Andalucía, March 31, 2026

scaletimedynamics.com
info@scaletimedynamics.com
Orcid | Academia | YouTube | Facebook

Version: 3.5

DIO: 10.5281/zenodo.19360353

SCALE-TIME THEORY

The Geometry of Scale-Space

ABSTRACT

Scale-Time Theory (STT) is a reconstruction framework in which spacetime, quantum behavior, and gravitation arise from a discrete readout acting on a pre-geometric substrate. The primitive arena is a spectral carrier defined on a punctured 2D scale plane Σ, evolving in a strictly monotone ordering parameter λ. A rotating dipole Source at the puncture injects conserved throughput via a constant area-flux law ς, generating outward Scale Flux and a truncated bipolar Fermat sweep: the two opposite source branches curve outward in a Fermat-spiral-like pattern whose cumulative spectral burden grows as ρ^2 (universally, with a prefactor set by the architecturally fixed source profile). The Master Sampler ignites at the first ring ρ_0 where this cumulative burden exceeds the threshold for continuous readout. The pre-MSS pattern is therefore a short, phase-dense bipolar sweep: ignition is driven by the cumulative spectral burden (growing as ρ^2), which reaches the representational crisis well before the pattern extends over a large radial range. At ignition, pointwise interpretation becomes ill-posed and the Master Sampler ignites at this ring as the minimal discrete structure that restores readable output.

The Master Sampler is operationally a scale-ring sampler at the ignition boundary. Its sole input is the ring-trace arrival signal: the regularized angular trace of the carrier approaching the MSS ignition ring from inside ($\rho \to \rho_0^-$). At each tick, this arrival waveform is decomposed by angular projection into discrete complex coefficients. These coefficients are distributed across a pre-alias three-dimensional spectrum via a fixed architectural lift map, then alias-summed into stored bins on the representable band. Physical reality is produced each tick by inverse Fourier synthesis on a reconstructed cubic lattice with finite lattice cutoff. The first sampled band edge beyond ignition, the Nyquist–Shannon Scale-Ring σ_1, is the maximally aliased regime; STT hypothesizes that this band is the home of the neutrino sector.

Once the sampler exists, time is defined operationally as a tick cadence, space as a finite-resolution lattice, and observables as inverse-Fourier synthesis from discretized spectral bins. Because sampling is filterless, aliasing is structural; the resulting non-injective readout and its Fourier uncertainty bound are identified as the origin of quantum indeterminacy. A scale-dependent oversampling ratio $\mathrm{OSR}(\sigma)$, constrained by fixed per-slice render capacity, yields a scale clock linking the quantum–classical transition to sampling depth (low OSR near the representational edge, high OSR on stable scale-harmonic structures).

The sampler's internal reconstruction operates as a full bipolar reconstruction cycle (q_+, q_-), the post-MSS continuation of the pre-geometric dipole source. The geometric field, gravity, lensing, and curvature, is sourced by the total burden of this full cycle. Observable proper time, however, is measured only in the q_+-projected readout sector, which registers one effective phase per full bipolar cycle. This sector-clock architecture, in the linearised symmetric bipolar regime, conditionally yields a factor-of-two between the geometric depth s_{geom} that shapes spacetime and the observer depth s_{obs} that governs clocked observables.

In this picture, gravity and time dilation emerge from render-cost–induced scale-upshift (scale-upshift $\rightarrow$ Scale-Flux slowdown $\rightarrow$ clock slowing), while dark-matter phenomenology is decomposed into two layers: a universal hidden co-burden from the full bipolar cycle, and a scale-dependent enhancement from scale-clock running in high-σ systems. Part 1 develops the conceptual foundation and interpretive claims; Part 2 provides the formal definitions, derivations, and calibrations needed to operationalize the framework, supported by a symbol reference.

Table of Contents

Abstract **2**
PART 1 Conceptual Framework **9**
1 INTRODUCTION: WHY NOT UNIFICATION? **9**
1.1 The Persistence of the Divide 9
1.2 A Different Diagnosis 9
1.3 The Role of the Master Sampler (MSS) 9
1.4 Scope and Structure of Part 1 10
1.5 The Canonical Mapping: Ring-Trace Promotion 10
2 CONCEPTUAL VOCABULARY **12**
3 THE PRE-MSS SETTING: BEFORE SPACE AND TIME **14**
3.1 The Scale Plane 14
3.2 The Ordering Parameter 14
3.3 The Dipole Source 14
3.4 The Conserved Constant Varsigma 15
4 SCALE FLUX AND THE UNAVOIDABLE FREQUENCY RAMP **16**
4.1 Outward Propagation in Scale 16
4.2 Why the Ramp Is Unavoidable 16
4.3 The Scale-Flux Velocity Law 16
5 THE DISTRIBUTION LIMIT AND MASTER SAMPLER NUCLEATION **17**
5.1 The Crisis: When Readout Fails 17
5.2 Master Sampler Ignition 17
5.3 The Scale Coordinate: The Render Index 17
5.4 A Crucial Onset Condition: No Anti-Alias Filter 18
5.5 The Render Capacity Postulate 18
6 INTERNAL CLOSURE, THE RECONSTRUCTION CYCLE, AND DM **19**
6.1 Why an Internal Closure Limit Is Needed 19
6.2 The Octonionic Closure Limit 19
6.3 The Full Bipolar Reconstruction Cycle 20
6.4 What the Two Sectors Are (and What They Are Not) 20
6.5 Dark Matter as a Two-Layer Effect 21
6.6 The Counter-Phase Sector and Its Cosmological Role 23
6.7 Connection to Gravity, Scale Lensing, and Forces 23
6.8 Qualitative Expectations 24
7 FOURIER READOUT: HOW FREQUENCY BECOMES PHYSICAL SPACE **25**
7.1 Why Fourier Synthesis Appears 25
7.2 What the Sampler Does, Tick by Tick 25
7.3 Why Aliasing Is Structurally Unavoidable 26
8 THE FIRST SAMPLED SCALE: THE NYQUIST–SHANNON SCALE-RING **27**
9 THE OVERSAMPLING RATIO: DERIVED FROM SCALE-FLUX SLOWDOWN **28**
9.1 OSR as a Consequence, Not a Postulate 28
9.2 The Two Regimes 28
9.3 One Architecture, Two Faces 28

9.4 What "Clean Readout" Means, and a Link to Known Constants 29
10 SCALE-HARMONIC RINGS: WHERE CLASSICAL REALITY ANCHORS 30
10.1 Harmonic Alignment with the Bipolar Structure 30
10.2 Alias-to-DC Phase-Lock 30
10.3 Classical Stability Is Not Generic 30
11 THE SCALE CLOCK AND TIME DILATION 31
11.1 Proper Time as Scale-Flux Rate 31
11.2 The Sector-Clock Architecture 31
11.3 Scale-Upshift: The Universal Cause of Time Dilation 32
11.4 The Equivalence Principle in STT 32
11.5 Connection to OSR 33
12 THE SCALE-RING LADDER: NAMED SCALES AND COSMIC EPOCHS 34
12.1 Cosmic History as a Scale-Ring Ladder 34
12.2 The Big Bang as a Boundary Outside Coordinate Time 34
12.3 The Named Scale-Rings 34
13 THE OBSERVER AS NESTED SCALES: ROAM VERSUS ANCHOR 35
13.1 From Single Scale-Ring to Nested Stack 35
13.2 Anchor Bands: Storage and Execution 35
13.3 The Roam Band: Exploration and Novelty 35
13.4 The Roam-to-Anchor Cycle 35
14 WHEEL KINEMATICS: STROBOSCOPIC ARTIFACTS OF SAMPLING 36
15 FORCE EMERGENCE: SAMPLER STRUCTURE 37
15.1 Photons and the Bridge Constant c_x 37
15.2 Electromagnetism: Neighbor-Scale Phase Transport 37
15.3 Gravity: Render-Cost Latency, Scale-Upshift, and Emergent Geometry 38
15.4 The Force Emergence Ladder 38
16 SCALE LENSING: GRAVITY AS OPTICS IN THE SCALE DIMENSION 39
16.1 Beyond Spatial Bending 39
16.2 The Mechanism in One Chain 39
16.3 What Scale Lensing Does 39
16.4 Lens Depth: A Compact-Object Taxonomy 40
16.5 Pulsars as Scale-Lensing Beacons 41
16.6 Black Holes as the Extreme: The Readout Horizon 41
17 SAMPLER EVOLUTION, EPOCH-DEPENDENT c_x, AND REDSHIFT 42
17.1 The Master Sampler Evolves with Scale Flux 42
17.2 Two Evolution Modes: Drift and Scale-Leaps 42
17.3 Cosmic Redshift as Epoch Mismatch 42
17.4 Unifying Cosmic, Gravitational, and Accelerative Redshift 42
17.5 Sampler Evolution and the Stability Landscape 42
17.6 A Discipline Constraint 43
18 SCALE-DRIVEN EVOLUTION IN FOUR DIMENSIONS 44
18.1 Scale Drift: The Moving Envelope Behind Ordinary Evolution 44
18.2 Scale-Leaps: New Stable Possibilities Without Visible Intermediates 44
18.3 Cambrian-Type Bursts 44

18.4 Connection to the Roam-Anchor Architecture 45
19 PARTICLE ONTOLOGY: STABLE READOUT KNOTS 46
20 SCALE COHERENCE AND THE RENDER STRESS TENSOR 48
20.1 Scale Coherence: Consistency Across the Scale Dimension 48
20.2 Why a Scalar Is Not Enough 48
20.3 The Render Stress Tensor: What It Tracks 48
20.4 The Scale Coherence Rule: Conservation Generalized to Include σ 48
20.5 OSR Inside the Tensor Picture: Laminar versus Turbulent 48
20.6 What This Enables (Without Committing to Specific Equations) 48
20.7 Render Burden Density and Burden Currents 49
20.8 Continuity of Coherence 49
21 DRAG, VISCOSITY, AND FLOW REGIMES IN A FILTERLESS SAMPLER 50
21.1 Why Drag Appears 50
21.2 OSR as the Viscosity Dial 50
21.3 Laminar versus Turbulent Readout 50
21.4 Drag in the Render Stress Picture 50
21.5 When Motion Outruns Sampling 50
21.6 Galaxy versus Solar System: Different Flow Regimes at Different σ 50
22 THE BOHR RADIUS: FIRST QUANTITATIVE CONTACT 52
22.1 The Starting Point: What a Filterless Sampler Cannot Do 52
22.2 Linking OSR to the Fine-Structure Constant via a Velocity Ratio 52
22.3 The Bohr Radius as Compton Length Times OSR 52
22.4 What the Fine-Structure Constant Means in STT 52
22.5 Clean Readout: An Operational Definition 52
22.6 Status and Scope 53
23 THE KALUZA–KLEIN PHASE-FIBER VIEW 54
23.1 The Full STT Coordinate Structure 54
23.2 Scale Slices as Preferred 4D Bands 54
23.3 Electromagnetism as Geometry of the Phase Fiber 54
23.4 Charge Quantization as Phase-Winding Number 54
23.5 Gravity and the Scale-Upshift Field 55
23.6 Why the Phase-Fiber View Is Useful 55
24 SUMMARY 56
25 GLOSSARY PART 1 58
PART 2 Mathematical Formalism 65
26 INTRODUCTION TO PART 2: THE DERIVATION LAYER 65
26.1 Epistemic Status (Strict) 65
26.2 What Part 2 Locks Down 65
27 NOTATION AND MATHEMATICAL PRELIMINARIES 67
27.1 The Pre-MSS Arena 67
27.2 Post-MSS Effective Coordinates 67
27.3 Fourier Conventions 67
27.4 Core Constants Reference 67
27.5 Convention on $\hbar$ 67

27.6 Ignition-Slice Convention 67
28 PRE-MSS CARRIER AND DIPOLE SOURCE 68
28.1 The Carrier Field 68
28.2 The Rotating Dipolar Boundary Drive 68
29 SCALE FLUX AS CONSTANT THROUGHPUT: MINIMAL EXPLICIT LAW 71
29.1 Constant Area Flux 71
29.2 Radial Slowdown 71
29.3 The Conserved Pre-MSS Constant ς 71
30 THE UNAVOIDABLE PHASE-CROWDING RAMP 72
30.1 Cumulative Spectral Burden 72
30.2 Ramp as Cumulative Burden Growth 72
31 DISTRIBUTION LIMIT AND MSS IGNITION 74
31.1 Representability Threshold 74
31.2 Ignition Condition 74
31.3 Operational Meaning of the Distribution Limit 74
31.4 The Regularized Pre-Limit Trace 75
31.5 Bridge to Post-MSS Readout 75
32 MSS ARCHITECTURE: TICKS, CELLS, BINS, AND FOURIER READOUT 76
32.1 Ticks and Lattice 76
32.2 Nyquist Binning Without Anti-Alias Filtering 77
32.3 Inverse Fourier Synthesis 78
33 ALIASING AS STRUCTURAL NON-INJECTIVITY 79
33.1 Aliasing Equivalence Classes 79
33.2 The Fourier Uncertainty Bound (Base Theorem) 79
34 UNITARY TICK UPDATE AND PHOTON DISPERSION 80
34.1 Unitary Fourier-Domain Evolution 80
34.2 Massless Lattice Dispersion and Maximal Speed c_x 80
34.3 Spherical Wavefronts and the Photon's σ-Envelope 80
35 CARRIER EVOLUTION AND THE SCHRÖDINGER LIMIT 82
35.1 Quadratic Spectral Phase Evolution (Massive Sector) 82
35.2 Bridge to Far-Field Reference Time 82
35.3 Clock Structure: Baseline Tick Time, Far-Field Time, and Local Proper Time 82
36 RENDER INDEX, SCALE CLOCK, AND OSR 84
36.1 Mapping Scale Depth to Render Index 84
36.2 Minimal Explicit Slowdown Law 84
36.3 OSR Definition 84
36.4 Scale-Upshift Field: Geometric and Observer Depths 84
37 CLOSURE AND THE BIPOLAR RECONSTRUCTION CYCLE 86
37.1 Internal Closure Cap and State Space 86
37.2 Bipolar Reconstruction Cycle 86
37.3 Bipolar Equipartition 87
37.4 Stationary Burden Symmetry 87
37.5 The Sector-Clock Theorem (Conditional Derivation) 88
38 THE KALUZA–KLEIN PHASE-FIBER MODEL: U(1) FROM SCALE PHASE 90

38.1 Compact Scale-Phase Coordinate 90
38.2 KK Metric Ansatz 90
38.3 Mode Number and Charge Quantization 91
39 RENDER STRESS TENSOR AND SCALE-COHERENCE CONSERVATION 92
39.1 Render Stress Tensor on $3 + 1 + \sigma$ 92
39.2 Scale Coherence as Continuity 92
39.3 Captured vs. Churn Split (Structural Refinement) 92
40 GRAVITY AS SCALE-UPSHIFT: WEAK-FIELD SKELETON 93
40.0 Burden Density and Enclosed Mass Notation 93
40.1 Minimal Scale-Upshift Action 93
40.2 Newtonian Matching as Calibration 94
40.3 Weak-Field Vacuum Solution 94
40.4 Time Dilation: Weak-Field Matching 95
40.5 Strong-Field Regime (Status) 96
40.6 Lens-Depth Parameter (Formal Definition) 96
41 DRAG AND FLOW REGIMES AS OSR-DEPENDENT CLOSURE 97
42 HYDROGEN RING CALIBRATION: α, OSR, AND THE BOHR RADIUS 98
42.1 Hydrogen OSR Identification 98
42.2 Bohr Radius as OSR Inflation of a Base Length 98
43 REDSHIFT AS METRIC MISMATCH 99
43.1 Gravitational Redshift from the Clock Law 99
43.2 Cosmic Redshift as Epoch Mismatch 99
43.3 Unification of Redshift Types 99
44 DARK MATTER: TWO-LAYER EFFECTIVE FORM 101
44.1 Hidden Co-Burden from the Full Bipolar Cycle 101
44.2 Scale-Clock Enhancement 101
44.3 Combined Effective Gravitational Response 102
44.4 Rotation Curves as the Structural Target 102
45 COMPLETION LAYER BOUNDARY 103
46 GLOSSARY OF PART 2 FORMAL OBJECTS 105
46.1 Axioms 105
46.2 Postulates 106
46.3 Calibration Hypotheses 106
46.4 Derived Results and Theorems 106
46.5 Key Formal Objects 107

PART 1 Conceptual Framework

1 INTRODUCTION: WHY NOT UNIFICATION?

1.1 The Persistence of the Divide

For nearly a century, theoretical physics has pursued a single goal with remarkable consistency: unify quantum mechanics and general relativity into one coherent theory. String theory, loop quantum gravity, causal set theory, and numerous other programs all share this premise, that a more complete formalism exists which reduces to quantum mechanics in one limit and to general relativity in another.

Yet every approach encounters the same structural tension. Quantum theory is usually formulated with an external time parameter and a fixed causal/background structure that defines evolution and localisation; the evolution itself is unitary, while probabilities enter only through outcome statistics, the Born rule. General relativity, by contrast, makes the spacetime geometry itself dynamical, so the friction between the two frameworks is largely about how "time" and "observables" are operationally defined when the geometry is not a background. The two theories do not merely disagree about details; they disagree about what the stage is made of and how the actors move on it.

1.2 A Different Diagnosis

STT takes a different starting point. The problem is not that we lack a bridge between two valid descriptions. The problem is that both descriptions are downstream readouts of a deeper system, and their apparent incompatibility is the expected outcome when two different operating regimes of that system are mistaken for independent theories.

The deeper system is a spectral carrier on a pre-geometric scale plane. Its intrinsic dynamics, outward Scale Flux, growing cumulative spectral burden, representational crisis, force the ignition of a discrete reconstruction mechanism: the Master Sampler, a scale-ring sampler at the critical boundary. Once the sampler exists, its output naturally produces what we recognize as quantum mechanics at low oversampling and general relativity at high oversampling, not because two theories are unified, but because both emerge from the same architecture under different sampling conditions.

1.3 The Role of the Master Sampler (MSS)

The Master Sampler is the central constructive object in STT. It is introduced as the minimal structure that restores well-defined readout after the carrier's growing cumulative spectral burden drives a representational crisis. Its ignition locus is the critical scale ring at ρ_0, a ring boundary, not a filled region, and its operational input is the regularized angular trace of the

carrier approaching that ring from inside. Once operational, it defines discrete time (ticks), discrete space (a lattice of cells), and a spectral-to-spatial conversion procedure (Fourier readout). STT identifies this aliasing with the irreducible indeterminacy of quantum mechanics, and the performance cost of maintaining persistent structure within the sampler with the geometric phenomena of general relativity.

The Master Sampler is introduced formally in Section 5. Every use of the term before that point refers to this same object: the scale-ring sampler whose ignition marks the origin of spacetime.

1.4 Scope and Structure of Part 1

Part 1 is concept-first and self-contained; it uses only a small number of orienting formulas, with no extended algebraic manipulation required. Section 2 presents the conceptual vocabulary. Sections 3–5 develop the pre-spacetime regime and the ignition event. Section 6 introduces the sampler's internal closure constraints, the full bipolar reconstruction cycle, and the two-layer account of dark matter. Sections 7–10 describe the post-ignition reconstructed world and its stability structure, including the derivation of the oversampling ratio from Scale-Flux slowdown. Section 11 develops the unified account of time dilation, including the sector-clock architecture that distinguishes geometric depth from observer depth. Sections 12–19 address the scale-ring ladder, the observer, kinematics, forces, scale lensing, sampler evolution, biological evolution, and particle ontology. Section 20 introduces scale coherence and the render stress tensor as the scaffolding for Part 2's field equations. Section 21 develops the drag, viscosity, and flow-regime interpretation of the tensor's behavioral signatures. Section 22 presents the Bohr radius as STT's first quantitative contact with known physics. Section 23 presents the Kaluza–Klein phase-fiber reformulation. A glossary of all defined terms closes the document.

Part 2 provides a derivation-layer formalization of this framework: each major claim is either derived explicitly or tagged as a calibration hypothesis or completion-layer item.

This manuscript does not claim that STT is already the final theory of everything. Its claim is narrower: that the Scale-Time approach identifies a plausible structural route for relating quantum behavior, spacetime, and gravitation, and that this route admits a genuine mathematical formalization rather than remaining at the level of metaphor or intuition.

1.5 The Canonical Mapping: Ring-Trace Promotion

STT is organized around a strict "before/after" split at Master Sampler ignition. To prevent ambiguity about what the sampler transforms and what it produces, the following canonical mapping governs the entire framework. Formal definitions and equations for each stage are given in Part 2, §32.

I. **Pre-MSS (continuous carrier evolution):** A complex carrier amplitude lives on the punctured 2D scale plane, evolving under a strictly monotone ordering parameter λ

that supplies before/after sequence only (no coordinate time or metric). Physical fields do not yet exist.

II. **MSS ignition (distribution limit):** At the ignition ring ρ_0, the cumulative spectral burden of the source-written carrier exceeds the threshold for continuous readout; the Master Sampler ignites at this ring boundary as the earliest discrete architecture that restores readable output. The post-MSS render index σ is anchored so that the ignition slice σ_0 has coordinate value $\sigma_0 \equiv 0$.

III. **Post-MSS (discrete reconstruction):** The sampler's sole causal input from the pre-geometric regime is the ring-trace arrival signal: the regularized angular trace of the carrier approaching the MSS ignition ring from inside ($\rho \to \rho_0^-$), sampled at tick times, then decomposed by angular projection into complex coefficients, lifted to a 3D pre-alias spectrum, alias-summed into stored bins, and finally inverse-Fourier synthesized into a reconstructed field on the spatial lattice. The full bipolar reconstruction cycle (q_+, q_-) operates at each tick. Observable 4D physics is read out from the q_+-projected sector.

IV. **Physical output (effective fields):** The reconstructed field $\psi_n(x)$, its Fourier-domain update law, and the emergent metric and connection in the $3 + 1 + \sigma$ effective package are the operational content of STT's "physical world."

2 CONCEPTUAL VOCABULARY

This section provides intuitive orientation for the central terms that will be defined precisely in the sections that follow.

Scale plane: The pre-existing arena, a punctured 2D surface on which spectral content is organized. Not physical space.

Ordering parameter (λ): A bare before/after sequence. Not time; just succession.

Dipole source: A steady, rotating bipolar seed at the puncture of the scale plane. Formally a puncture-centered bipolar drive; intuitively visualized as a yin-yang-like rotating double core, a coherent two-lobed phase exciter, not two independent objects. In signal-processing terms: a balanced rotating phase transmitter writing an angular waveform into an outward channel. Generates a truncated bipolar Fermat sweep. The pre-geometric ancestor of the post-MSS bipolar reconstruction cycle.

Scale Flux: Radial outward propagation of the carrier on the scale plane, from small to large scale depth. The primary "arrow" of the theory.

Frequency ramp: The growing cumulative spectral burden caused by steady bipolar rotation being written into an outward-propagating carrier. Not a local-wavenumber effect (the local phase gradient decreases outward), but a cumulative-inventory effect: the spectral burden grows as $\chi_H \, \rho^2$, where the ρ^2 scaling is universal and the prefactor depends on the architecturally fixed source profile.

Distribution limit: The point where readout fails, the cumulative spectral burden at the ignition ring exceeds the threshold for continuous representation. The trigger for everything that follows.

Master Sampler (MSS): The discrete reconstruction mechanism that ignites at the critical scale ring ρ_0. Operationally a scale-ring sampler: its input is the regularized angular trace of the carrier approaching the ignition ring from inside, not the whole scale plane. Defines ticks, cells, bins, and Fourier readout. The origin of spacetime.

Full bipolar reconstruction cycle (q_+, q_-)**:** The post-MSS continuation of the pre-geometric dipole source. A two-phase sourcing architecture in which both sectors contribute to the total reconstruction burden. The geometric field is sourced by the full cycle.

q_+**-projected observer sector:** The readout channel from which observable proper time and electromagnetically visible physics are measured. Registers one effective phase per full bipolar cycle.

Geometric depth (s_{geom}): The full-cycle scale-upshift field. Sources geometry, gravity, and lensing.

Observer depth (s_{obs}): The projected-sector scale-upshift governing measured clock slowdown. In the linearised symmetric bipolar regime, related to geometric depth by $s_{\text{geom}} = 2\, s_{\text{obs}}$ (Conditional Result C7).

Oversampling ratio (OSR): How far from the representational edge the system sits. High OSR $\rightarrow$ classical; low OSR $\rightarrow$ quantum.

Scale clock: The local Scale-Flux rate that sets a system's time rate. Proper time is a readout of the scale clock, measured in the q_+-projected sector.

Scale-upshift: A shift toward higher effective scale. Produces Scale-Flux slowdown and time dilation. The universal cause of gravitational and accelerative clock slowing.

Render stress tensor: The bookkeeping object tracking render burden density, spatial flow, directional stresses, and coherence transport along σ.

3 THE PRE-MSS SETTING: BEFORE SPACE AND TIME

3.1 The Scale Plane

The starting point of STT is a punctured two-dimensional surface $\Sigma = \mathbb{R}^2 \backslash \{0\}$, the scale plane. In polar coordinates (ρ, ϕ), $\rho > 0$ measures radial distance from the puncture and $\phi \in [0, 2\pi)$ is the angular coordinate.

This plane is the only pre-existing substrate. It is not embedded in a higher-dimensional space. It does not presuppose geometry. It is the minimal arena on which spectral content can be organized and from which all subsequent structure will be derived.

3.2 The Ordering Parameter

Evolution on the scale plane is tracked by a strictly increasing ordering variable λ. This parameter supplies only an internal "before/after", a bare sequential ordering with no metric, no rate, and no external clock. It is the most primitive notion of progression: things happen in sequence, but there is no time in which they happen.

3.3 The Dipole Source

At the puncture of the scale plane, a steady bipolar source rotates as the ordering parameter advances. This is the coherent seed of the entire theory: a persistent, directed write orientation that gives the carrier a stable bias. Without it, the carrier would have no preferred direction of spectral inscription and no basis for the structures that later emerge.

The source is best understood at three levels:

At the **foundational formal level**, it is a rotating bipolar puncture drive: two opposite phase-amplitude lobes co-rotating at the origin, inscribing a bipolar pattern into the outward-moving carrier. This is the object defined by Axiom A2 in Part 2.

At the **geometric-visualization level**, it may be pictured as a yin-yang-like rotating bipolar core: two counterposed phase centers within an infinitesimal source region, each carrying opposite phase bias. This finite-core image captures the essential morphology, two interlocking halves of a single rotating whole, while the formal theory works in the zero-core (puncture) limit of this picture. The yin-yang image is topological and dynamical, not material: it denotes a coherent two-lobed phase source, not two literal bodies orbiting in pre-space.

At the **operative-consequence level**, what matters is that the source continuously writes rotated bipolar phase into the outward carrier, producing a truncated bipolar Fermat sweep. The two opposite branches immediately curve outward in a Fermat-like pattern because the source keeps rotating while its inscription is being carried away from the puncture. The Master Sam-

pler ignites early enough that the pre-MSS pattern does not need to accumulate many visible wraps. What exists before ignition is not a vast spiral archive with many completed turns, but a short, phase-dense outward inscription whose spiral tendency is already present and already sufficient to generate increasing cumulative spectral burden.

Signal-processing interpretation. In signal-processing terms, the dipole source functions as a balanced rotating phase exciter, a coherent two-phase rotor whose opposite lobes remain phase-linked while the whole pattern rotates. It writes a structured angular waveform into the outward-propagating carrier. The outward Scale Flux is the transport channel. The MSS ring is the first receiver boundary at which that waveform must be discretely sampled because its cumulative spectral burden has exceeded the limit of continuous readout. The Master Sampler does not read two orbiting objects; it reads the angular trace of this rotating bipolar phase source at the first critical ring where continuous representation fails.

The dipole source is therefore best understood as a rotating bipolar phase topology whose ring-trace, not any putative pre-geometric "objects", is what the Master Sampler first receives and discretizes.

The dipole source is the pre-geometric original of the bipolar architecture. After MSS ignition, this same bipolarity survives as the full bipolar reconstruction cycle, the two-phase sourcing structure from which geometry is built. The dipole source is not retired at ignition; it is promoted into the operational core.

3.4 The Conserved Constant Varsigma

The pre-MSS regime has two steady drives: a throughput rate (how much spectral content is rendered per unit of the ordering parameter) and the source-phase rotation rate. Their ratio defines a conserved constant ς, varsigma, that sets the carrier's "write geometry." This constant is not adjustable after the fact; it fixes, once and for all, the relationship between spectral growth and source orientation, and thereby determines where stable sampling can later emerge.

The bipolar source profile, the specific angular shape of the rotating two-lobed pattern, is fixed architecturally as part of the source's structural identity. Given that fixed profile, ς is the single free parameter of the pre-MSS regime. A richer source profile (one with more harmonic content) accumulates spectral burden faster, shifting the ignition radius quantitatively, but the quadratic growth law and the inevitability of ignition are universal.

4 SCALE FLUX AND THE UNAVOIDABLE FREQUENCY RAMP

4.1 Outward Propagation in Scale

STT posits an intrinsic Scale Flux: the carrier continually propagates outward, from smaller to larger scale depth, along the radial coordinate of the scale plane.

This is not motion through physical space; there is no physical space. It is a directed flow along the scale coordinate, analogous to a signal propagating along a waveguide: the carrier moves outward because the theory's dynamics are scale-directed, not spatially directed.

4.2 Why the Ramp Is Unavoidable

The frequency ramp is not a local-wavenumber effect, the local phase gradient at any single radius actually decreases outward as the carrier spreads over a larger frontier. The ramp is the steady growth of cumulative spectral burden: the total spectral inventory inscribed in the carrier up to each radius.

Because the outward flux slows with radius (the flux velocity goes as $1/\rho$), the carrier spends more ordering-parameter time crossing each successive radial increment. During that longer transit, the rotating source writes more spectral content. The cumulative spectral burden therefore grows as ρ^2, faster than the frontier grows. This is the unavoidable frequency ramp: a relentless accumulation of spectral inventory that eventually overwhelms any continuous readout, even over a short radial extent. The ρ^2 scaling is universal for any bipolar source; the detailed source morphology affects only the prefactor.

The outward scale arrow is STT's primary ordering. It is an arrow in scale, not an arrow in coordinate time. Coordinate time does not exist yet.

4.3 The Scale-Flux Velocity Law

Scale Flux is not only directional; it also decelerates with increasing scale depth. The Scale-Flux Velocity Law is the named principle expressing this: the effective rate of Scale Flux decreases with increasing render index σ, because each σ-slice has fixed render capacity and larger-scale coherence boundaries require more processing. This deceleration is a defining feature of the theory: it ensures that larger scales are explored more slowly, and it is the single primitive from which the oversampling ratio and the scale clock will both be derived.

5 THE DISTRIBUTION LIMIT AND MASTER SAMPLER NUCLEATION

5.1 The Crisis: When Readout Fails

MSS ignition is not triggered by the local wavenumber at the ignition ring being high, the local wavenumber actually decreases outward. It is triggered by the cumulative spectral burden reaching a critical threshold. The spectral inventory that the rotating source has written into the carrier grows as ρ^2, and at ρ_0 this cumulative load exceeds what any continuous readout can faithfully represent. The output becomes distributional rather than function-valued. This is the distribution limit, and it is the causal trigger for everything that follows.

5.2 Master Sampler Ignition

The ignition ring ρ_0 is the first radius where the cumulative spectral burden of the source-written carrier exceeds the threshold for continuous readout. At that boundary, the system switches architecture. A discrete reconstruction mechanism, the Master Sampler, ignites. It introduces discrete time (ticks), discrete space (cells), and a spectral-to-spatial conversion procedure (Fourier readout). This ignition is the origin of spacetime.

The MSS is a scale-ring sampler whose ignition locus is the critical ring at ρ_0 (equivalently $\sigma = 0$). Its operational input is the regularized angular trace of the carrier approaching that ring from inside ($\rho \to \rho_0^-$; see §31.4): it reads the angular structure arriving at the approach to a single ring. Everything inward of ρ_0 is pre-MSS carrier; everything outward is post-MSS reconstructed lattice. The ring itself is the interface, a boundary, not a filled region, and not a transformation of the whole scale plane.

The Master Sampler is the earliest discrete architecture capable of stabilizing what the dipole source has already made unavoidable. The pre-MSS regime is therefore shorter, cleaner, and more immediate than a picture of extended spiral winding would suggest: the dipole seeds a bipolar spiral tendency immediately, the carrier accumulates increasing spectral burden, and the sampler ignites early, before extended visible winding accumulates.

5.3 The Scale Coordinate: The Render Index

Post-MSS, the radial direction on the scale plane is re-expressed as a dimensionless render index $\sigma := \ln(\rho/\rho_0)$, with the ignition slice $\sigma_0 \equiv 0$ and σ increasing outward. The render index is not merely a radial label; it measures how much coordination the sampler must perform to maintain a stable 4D readout at that scale. Higher σ means higher render cost, slower scale clock, and (on stable bands) higher OSR.

5.4 A Crucial Onset Condition: No Anti-Alias Filter

The Master Sampler ignites without an anti-alias filter. No pre-filter exists that could smooth the carrier before sampling begins, the carrier is the raw input, and the sampler is the first discrete structure. Aliasing is therefore structurally unavoidable from the first tick onward. This is not a design flaw; it is the origin of quantum indeterminacy in STT.

5.5 The Render Capacity Postulate

The Scale-Flux Velocity Law, stated qualitatively above, acquires a concrete operational form post-ignition:

Render Capacity Postulate: Each σ-slice has a fixed total render capacity per cycle, a bounded amount of coherent updating the Master Sampler can perform per slice, per tick.

Coherence maintenance cost scales with the extent of what must be kept mutually consistent, practically, with the coherence boundary a system presents to the sampler: how many mutually coupled degrees of freedom must agree per update. As σ increases, this coherence boundary grows. With a fixed slice budget, the sampler responds by increasing latency: larger-scale systems take more cycles to process, so the effective scale clock slows.

This turns "bigger systems run slower" into a direct capacity-accounting statement and connects several threads already introduced:

OSR origin: When the scale clock slows, the sampler accrues more effective updates per meaningful change. This is more sampling per effective degree of change, exactly what OSR measures. Scale-Flux slowdown is therefore the physical origin of OSR.

Drag and viscosity: When coherence demand approaches budget limits, the system develops backpressure: the readout behaves like a medium with effective viscosity, because it cannot instantly reconcile all interactions. This is the alias-driven drag of Section 21.

Solar system versus galaxy: A solar system has limited global coordination surface (hierarchical dominance, few strong couplings) and fits comfortably in the slice's render budget, faster effective scale clock, less scale-running. A galaxy has enormous global coordination surface (many-body coupling, long-lived collective modes) and stresses the same budget, slower effective scale clock, stronger scale-dependent dynamics.

6 INTERNAL CLOSURE, THE RECONSTRUCTION CYCLE, AND DM

The Master Sampler ignites at σ_0 as the minimum structure needed to restore well-defined readout. But "minimum structure" is not "no structure": the sampler must adopt an internal bookkeeping system, rules for how phases, orientations, and cross-scale links combine and remain consistent under repeated reconstruction. This section describes the constraints on that bookkeeping, their minimal consequence for the reconstruction schedule, the resulting bipolar architecture, and the separate mechanism by which STT accounts for the dark matter inference.

6.1 Why an Internal Closure Limit Is Needed

For the sampler to remain stable, it must maintain consistent bookkeeping for phase, orientation (handedness, if any), cross-scale linking rules, and sectoring (if readout is not single-channel). This bookkeeping cannot be arbitrarily large or unconstrained, otherwise the sampler would not "close" on a stable set of rules and would re-enter the distributional instability it was created to solve.

That motivates a closure principle: the sampler's internal algebra must be finite, self-consistent, and rich enough to support the structures that follow (charges, interactions, persistent knots) but no richer than necessary.

6.2 The Octonionic Closure Limit

Postulate: At MSS ignition, the sampler adopts a minimal nontrivially closed internal bookkeeping structure. The cap on independent internal directions it can stably maintain is eight, an octonionic closure limit.

In plain language: the sampler has an internal "state algebra" that governs how phases and internal directions combine during reconstruction. The octonionic limit means: the smallest stable closure with enough richness to support sectoring, interactions, and consistent cross-scale linking is an eight-direction basis. This is a stability constraint, not a claim that octonions explain all of particle physics. It caps the number of independent internal channels the sampler can instantiate.

What this buys immediately: a principled reason why STT produces a small, structured set of persistent sectors and modes rather than an unbounded zoo. It provides a natural scaffold on which later structure (charge families, coupling constants, species) can be built without committing to a full mapping at the foundation layer.

6.3 The Full Bipolar Reconstruction Cycle

Once an internal closure bound exists, it constrains the reconstruction schedule. The simplest nontrivial sectoring that preserves stable reconstruction, allows a conjugate channel, and avoids forcing all persistent structure into a single readout phase is a two-phase architecture.

Postulate (Full Bipolar Reconstruction Cycle). The sampler reconstructs reality through a full bipolar cycle (q_+, q_-) per tick:

- q_+ **sector**, the readout channel that defines our electromagnetically visible 4D world. Observable proper time is measured here.
- q_- **sector**, a counter-phase readout channel, shifted in internal phase relative to q_+, with suppressed direct visibility in our electromagnetic reconstruction.

This two-phase structure is the post-MSS continuation of the pre-geometric dipole source. The pre-MSS source, a yin-yang-like rotating bipolar core continuously inscribing phase into the carrier, does not vanish at ignition. Its bipolarity is promoted into the sampler's operational core as the full bipolar reconstruction cycle, with q_+ and q_- as the post-ignition inheritors of the two counterposed pre-geometric phase lobes. Both sectors contribute to the total reconstruction burden.

Under the closure limit, the sampler's minimal stable way to host a counter-phase sector is this bipolar interleaving. One does not need to claim that octonions force exactly two sectors, only that the closure limit, combined with the requirement for stable sectoring, naturally supports the bipolar cycle as its simplest realization.

6.4 What the Two Sectors Are (and What They Are Not)

The q_+ sector is the set of reconstructed configurations that couple to the electromagnetic bookkeeping rules of our home slice. Visible matter and ordinary laboratory physics live here.

The q_- sector is a counter-phase reconstruction channel. It is dynamically real, it can host persistent structure, but it is not automatically visible in q_+ electromagnetic readout because coupling between sectors is suppressed by the phase offset.

An important distinction: laboratory antimatter (positrons, antiprotons, antihydrogen) is electromagnetically active and therefore q_+-sector physics, conjugate excitations within the visible readout. The q_- sector is not ordinary antimatter. It is a separate reconstruction channel whose EM visibility in our home sector is suppressed. This avoids contradictions with known particle physics.

6.5 Dark Matter as a Two-Layer Effect

With the sector-clock architecture in place, STT decomposes dark-matter phenomenology into two structurally distinct layers: a universal hidden co-burden from the full bipolar reconstruction cycle, and a scale-dependent enhancement from scale-clock slowdown. The first explains why the total geometric source exceeds the visible sector alone; the second explains why the apparent excess strengthens in high-σ systems such as galaxies and clusters.

Layer 1: Hidden co-burden from the full bipolar cycle.

The visible sector q_+ is not the whole system. Because geometry is sourced by the full bipolar reconstruction cycle, the total gravitating burden is:

$$B_{\text{tot}} = q_+ + q_-$$

The q_- sector contributes burden that is gravitationally active but not directly read out in ordinary q_+ electromagnetic observation. For stationary configurations respecting the bipolar symmetry, the hidden sector contributes burden equal to the visible one (Postulate P6). This does not mean STT simply predicts "double the matter" in a naive additive sense. It means that visible matter alone is not the correct source term for geometry. The observer sees one projected half of the cycle, while gravity responds to the whole cycle.

This is a universal hidden baseline: geometry is sourced by more burden than the observer directly sees, regardless of scale or environment.

Layer 2: Scale-clock slowdown as the variable enhancement.

The second layer is scale-clock running, the dependence of the effective gravitational response on the render index σ. The scale clock, the local Scale-Flux rate, slows with increasing σ (Section 4.3). Because σ measures render burden (Section 5.3), systems that require more global coordination to maintain a stable 4D readout sit at higher σ and therefore run on a slower scale clock. In higher-σ systems, the same visible baryonic content produces a stronger geometric effect because the reconstruction runs under different scale conditions.

This means the dark-matter-like excess is not constant across all systems. It grows with scale, complexity, and collective burden. Galaxies and clusters show more apparent excess than small, hierarchically simple systems.

This is a scale-dependent amplification, not a fixed hidden mass fraction, but an environmental enhancement that depends on render index.

The combined effective gravitational response is therefore schematically:

$$M_{\text{eff}} \sim \left(M_{q_+} + M_{q_-}\right) \Xi_\sigma$$

where M_{q_+} is the visible-sector burden, M_{q_-} is the hidden co-burden from the complementary sector, and Ξ_σ is the scale-clock enhancement factor. Under stationary burden symmetry (P6), $M_{q_-} = M_{q_+}$, so the total source is already twice the visible sector alone, and that total is then further modulated by the scale-clock factor.

Solar system versus galaxy: the render-index distinction. A solar system is largely hierarchical, one dominant mass and a relatively small number of bodies. Maintaining a consistent reconstruction is a comparatively low global coordination task, so the system sits at a lower system coordination index σ_{sys}, runs on a relatively faster scale clock, and the scale-clock enhancement Ξ_σ is near unity. A galaxy, by contrast, is a massively collective N-body structure with enormous global coordination surface. It sits at higher σ_{sys}, where Ξ_σ is significantly larger, producing the stronger effective gravitational response that is interpreted as "missing mass."

When we infer "mass" from galactic dynamics using constants calibrated in lower-σ_{sys} systems (solar-system physics), we implicitly assume the same system coordination index and the same sector-visibility apply. Neither assumption holds: the hidden co-burden is always present but not seen, and the scale-clock enhancement is stronger at galactic σ_{sys}.

Why the effect strengthens in galaxy outskirts: two distinct variables. Two different measures of reconstruction condition must be distinguished here:

The **system coordination index** σ_{sys} is the global render index of the system as a collective structure. A galaxy has high σ_{sys} because of its enormous coordination surface, this is what drives the scale-clock enhancement $\Xi_\sigma > 1$.

The **local stability margin** $\text{OSR}_{\text{local}}(r)$ is the oversampling ratio at a specific position within the system. In galaxy outskirts, low-density, low-acceleration regions, the local reconstruction approaches a stability edge: $\text{OSR}_{\text{local}}$ is low even though the system-level σ_{sys} is high.

These two variables can move in opposite directions: the system sits at high σ_{sys} (producing scale-clock enhancement), while outskirt positions have low $\text{OSR}_{\text{local}}$ (producing nonlinear render response near the stability edge). The combination, strong scale-clock enhancement acting on a region where the reconstruction is already near its representational limit, is what produces the strongest apparent dark-matter excess in galaxy outskirts. The result matches the observed pattern: stronger apparent dark matter effect in low-acceleration, low-density regions of high-σ_{sys} systems.

Formal status: Part 2's minimal rotation-curve form (§44.4) implements only the global Ξ_σ from σ_{sys}; the position-dependent interplay between σ_{sys} and $\text{OSR}_{\text{local}}(r)$ is a conceptual prediction of Part 1 whose formal implementation is completion-layer work.

Lensing: Because both layers, hidden co-burden and scale-clock enhancement, contribute to the total geometric source, gravitational lensing tracks the combined effective field. Lensing anomalies do not require a hidden substance; they follow from the full bipolar sourcing and the scale-dependent reconstruction geometry.

6.6 The Counter-Phase Sector and Its Cosmological Role

The q_- sector is not laboratory antimatter. Antiparticles created in laboratories (positrons, antiprotons, antihydrogen) are electromagnetically active and therefore belong to q_+-sector physics, conjugate excitations within the visible sector. The q_- sector is a separate readout-gate channel, mostly decoupled in EM visibility.

With the two-layer decomposition, the bipolar architecture now plays a direct cosmological role: its hidden co-burden is the first layer of dark-matter phenomenology. The q_- sector is no longer just an abstract partner channel, it contributes to the explanation of why geometry exceeds visible matter. At the same time, it retains its structural role as a counter-phase sector with principled conjugate bookkeeping under the octonionic closure limit.

The clean separation is: hidden co-burden (from the full bipolar cycle) provides a universal baseline of gravitating burden beyond the visible sector, while scale-clock enhancement (from the scale dimension's render-index dependence) provides the system-dependent excess that varies with σ and actually resembles observed dark-matter behavior across different astrophysical systems.

6.7 Connection to Gravity, Scale Lensing, and Forces

This section's two dark-matter layers connect to the existing force picture without replacing it:

Gravity remains render-cost–induced scale-upshift. The render load includes contributions from both q_+ and q_- sectors, gravity is sector-blind. The total burden sourcing geometry is $B = q_+ + q_-$, the full bipolar cycle. This is the structural origin of the hidden co-burden. The force emergence ladder (Section 15) gains this qualifier: gravity sums render cost from both sectors.

Scale-clock running adds a second gravitational effect on top of the full-cycle sourcing: the effective gravitational response itself depends on which scale band the system occupies. This is the scale-dependent amplification layer, and it is the origin of the environment-dependent dark matter inference at galactic and cluster scales.

Scale lensing remains cross-σ coupling enhancement. In strong-lens environments, both layers, hidden co-burden and scale-clock enhancement, contribute to lensing anomalies.

Electromagnetism remains neighbor-scale $U(1)$ phase transport, understood as the q_+-sector EM channel. The q_- sector has its own internal phase rules, but they do not couple directly to q_+ EM.

6.8 Qualitative Expectations

Without committing to quantitative predictions in Part 1, the framework supports several qualitative expectations:

Universal hidden baseline: Every gravitating system is sourced by the full bipolar cycle, not just the visible sector. The total geometric burden exceeds the visible burden in all environments, providing a universal floor of "excess" gravity relative to visible matter.

Scale-dependent gravitational response: Large-scale systems (galaxies, clusters) exhibit stronger effective curvature per unit baryonic load than small-scale systems (solar systems, binary stars), due to scale-clock enhancement on top of the hidden co-burden.

Low-acceleration enhancement: The scale-clock effect becomes most visible in low-density, low-acceleration outskirts where reconstruction approaches a stability edge.

Lensing without hidden substance: Gravitational lensing anomalies follow the combined effective field, full bipolar sourcing plus scale-clock geometry, requiring no additional substance.

Environment dependence: Deep scale lenses (compact objects, dense environments) produce the strongest cross-sector coupling, and therefore the strongest constraints on or rare signatures from the q_- sector.

7 FOURIER READOUT: HOW FREQUENCY BECOMES PHYSICAL SPACE

7.1 Why Fourier Synthesis Appears

The carrier's content is fundamentally spectral, organized as frequency components, not spatial patterns. Once the distribution limit forces the introduction of a discrete sampler, the system needs a regulated, universal procedure for converting spectral content into interpretable patterns. The simplest and most natural such procedure is Fourier synthesis: combining harmonic components, weighted by their amplitudes and phases, to produce a spatial field.

Fourier readout is not a mathematical convenience in STT. It is the readout mechanism, the process by which the physical world is produced.

7.2 What the Sampler Does, Tick by Tick

On each tick, the Master Sampler executes one full bipolar reconstruction cycle through the following stages:

First, it reads the ring-trace arrival signal: the regularized angular trace of the carrier approaching the MSS ignition ring from inside, sampled at the current tick's ordering-parameter step.

Second, it decomposes this arrival waveform by angular projection into discrete complex coefficients, one per rotor mode.

Third, the architectural lift map distributes these coefficients into a pre-alias three-dimensional spectrum that extends beyond the representable band.

Fourth, because no anti-alias filter is applied, this lifted spectrum is folded into the representable band by alias summation, producing the stored bins (filterless, no anti-alias gate).

Fifth, it combines the stored bin content, amplitudes and phases, via inverse Fourier synthesis to produce a field pattern across its lattice of spatial cells.

Both the q_+ and q_- sectors participate in this cycle. The full bipolar burden is what sources geometry. The q_+-projected output is what defines observable readout.

Each tick, the sampler "draws" physical space by synthesizing its stored harmonics into a reconstructed pattern. The next tick, it updates the bins and draws again. This repeated cycle of receive–project–lift–alias–synthesize is the heartbeat of post-MSS reality.

7.3 Why Aliasing Is Structurally Unavoidable

Because the sampler ignites without a filter, all spectral content beyond the Nyquist edge is folded back into the representable band. This is not a failure of design, it is the fundamental origin of quantum indeterminacy: multiple underlying spectral configurations produce identical readout, making the mapping from underlying reality to reconstructed physics non-injective.

8 THE FIRST SAMPLED SCALE: THE NYQUIST–SHANNON SCALE-RING

The first band sampled beyond the ignition ring is at half the MSS sampling rate, the σ_1 scale-ring, the Nyquist–Shannon Scale-Ring. This is the maximally aliased regime: the carrier is barely resolved, alias content is maximal, and reconstructed patterns are at their most ambiguous.

STT identifies this band with the neutrino sector. This is a structural placement: the neutrino is the first persistent pattern the sampler can maintain, at the very edge of representability, maximally alias-dominated, barely massive, weakly coupled. The neutrino's known properties, tiny mass, near-null transport, weak interactions, match the expected phenomenology of the maximally aliased first-sampled band.

9 THE OVERSAMPLING RATIO: DERIVED FROM SCALE-FLUX SLOWDOWN

9.1 OSR as a Consequence, Not a Postulate

The oversampling ratio is not an independent parameter. It is derived from the Scale-Flux Velocity Law: because Scale Flux decelerates with increasing scale depth, deeper-scale systems are sampled more times per meaningful change. OSR measures this margin.

9.2 The Two Regimes

Low OSR (fast Scale Flux, near the sampling edge): the system changes rapidly relative to the MSS cadence, leaving the reconstruction under-resolved, alias-dominated, and ambiguous. Readout is ambiguous, non-unique at the inverse-map level (yielding probabilistic outcome statistics), and interference-prone. This is the quantum regime.

High OSR (slow Scale Flux, deep safety margin): the system dwells in the band, alias residuals become negligible, reconstruction is stable, repeatable, effectively deterministic. This is the classical regime.

9.3 One Architecture, Two Faces

OSR replaces the traditional divide between "quantum" and "classical" with a continuous, position-dependent stability margin within one and the same architecture. There are no separate quantum and classical postulates. There is one sampling system, and the character of its output depends on how far from the representational edge it is operating, which is set by how fast Scale Flux is running at that scale depth.

This is the core of STT's answer to the unification problem: quantum mechanics and general relativity are not two theories requiring a bridge. They are the low-OSR and high-OSR behaviors, respectively, of a single reconstructive system, and OSR itself is derived from the single primitive of Scale-Flux rate.

STT is not offered as a substitute for decoherence. Decoherence is the objective, open-system dynamics that suppresses off-diagonal interference terms in macroscopic records; it is physics that happens regardless of any observer's resolution. STT's claim is different and complementary: because the sampler's reconstruction map is non-injective in the filterless case (formalised as Derived Result D3 in Part 2, §33.1), multiple underlying carrier configurations correspond to the same reconstructed readout. Decoherence then explains which reconstructed degrees of freedom become stable, classical records, it selects among the equivalence classes that aliasing creates. The two mechanisms operate at different levels of the architecture: aliasing sets the multiplicity, decoherence winnows it.

9.4 What "Clean Readout" Means, and a Link to Known Constants

A filterless sampler cannot eliminate aliasing; it can only make the alias residue small. In STT, that "smallness" is precisely what OSR measures. A practical intuition for the stability ladder:

OSR around 5–10: readout looks mostly stable and classical; alias signatures are present but not dominant. OSR around 20–50: alias artifacts are small compared to dominant reconstructed structure, a "clean" regime. OSR around 100 or above: extremely robust; alias residue is negligible unless probing very subtle effects.

A natural calibration hypothesis. OSR can be read as a velocity ratio: the fraction of the sampler's native null-transport speed (c_*) that survives as slow residual drift in the reconstructed sector. In atomic physics, typical electron speeds in hydrogen scale as the fine-structure constant times the speed of light. This suggests a clean identification:

At the hydrogen scale-ring, OSR is of order $1/\alpha \approx 137$.

10 SCALE-HARMONIC RINGS: WHERE CLASSICAL REALITY ANCHORS

10.1 Harmonic Alignment with the Bipolar Structure

Not all scale depths are equally stable. At certain bands, the sampler's resolution and the carrier's spectral structure come into particularly clean alignment, harmonic resonance across the full bipolar reconstruction cycle. At these bands, alias residuals collapse into slow, phase-locked residuals near DC. The result is enhanced classical stability: patterns persist, readout becomes repeatable, and the world looks solid.

These are Scale-Harmonic Rings, the special scale bands where classical reality anchors.

10.2 Alias-to-DC Phase-Lock

At a Scale-Harmonic Ring, the dominant alias modes are not wildly fluctuating; they phase-lock into slow residuals. The alias content is still there, it cannot be removed, but it becomes functionally inert: stable, repeatable, and effectively invisible to macroscopic observation.

10.3 Classical Stability Is Not Generic

Scale-Harmonic Rings are special. Between them, alias patterns can be rapidly varying, interference-prone, and unstable. Classical stability is not a default in STT, it is an earned property of particular scale bands where harmonic alignment conspires with Scale-Flux slowdown to suppress alias ambiguity.

11 THE SCALE CLOCK AND TIME DILATION

11.1 Proper Time as Scale-Flux Rate

Observable time in STT is operationally defined by the scale clock: the local rate of Scale Flux at a system's effective render index. Where Scale Flux runs fast (low σ), local time runs fast. Where Scale Flux runs slow (high σ), local time runs slow. Proper time is a readout of the scale clock, measured in the q_+-projected observer sector.

11.2 The Sector-Clock Architecture

The full bipolar reconstruction cycle is the sourcing mechanism for geometry. But the observer does not have access to the whole cycle at once.

Sector-Clock Principle. The geometric field is sourced by the full bipolar reconstruction cycle (q_+, q_-), while observable proper time is measured in the q_+-projected readout sector and therefore counts one effective phase per full bipolar cycle.

At a fixed scale position, the observer is locked to one projected half of the bipolar cycle, much as a fixed observer sees only one side of the Moon at a time. The hidden half is not absent; it remains part of the full structure and still contributes to the total geometric burden. The observer clocks only the visible half of the cycle, but geometry is sourced by the whole cycle.

This two-phase sourcing / one-sector observation split is not introduced ad hoc to repair a coefficient. It is the operational consequence of the bipolar architecture already present in the pre-MSS dipole source and retained in the post-MSS reconstruction. In Part 2 (§37.5), the specific factor-of-two is conditionally derived in the linearised symmetric bipolar regime from four explicit assumptions: bipolar equipartition (equal closure capacity), stationary burden symmetry (equal sector burdens), an observer source law (the q_+-projected clock responds to q_+-sector burden through the same render-cost operator), and shared linearised coupling and boundary conditions.

The sector-clock architecture produces two distinct versions of scale depth:

Geometric depth $s_{\text{geom}}(x)$: the full-cycle scale-upshift field. Sources geometry, gravity, lensing, and curvature. Responds to the total burden $B = q_+ + q_-$.

Observer depth $s_{\text{obs}}(x)$: the projected-sector scale-upshift governing measured clock slowdown. Counts one effective phase per full bipolar cycle. In the linearised symmetric bipolar regime (Conditional Result C7, Part 2 §37.5):

$$s_{\text{geom}} = 2\, s_{\text{obs}}$$

Geometry feels the full two-part cycle; the observer measures only one effective half-cycle.

11.3 Scale-Upshift: The Universal Cause of Time Dilation

Any mechanism that shifts a system to higher effective scale, a scale-upshift, slows the scale clock.

Gravity: Persistent captured structure (mass, energy, coherent configurations) imposes render load on the sampler. This load shifts the local system to higher effective scale (or equivalently reduces effective update capacity). Higher scale means slower Scale Flux, therefore a slower system clock. Gravitational time dilation is scale-upshift caused by render cost.

Acceleration: Accelerating a system forces additional scale involvement, maintaining coherent readout under changing motion requires the system to occupy higher-scale slices with greater transport overhead. This pushes the system into slower Scale Flux, reducing the rate of stable readout updates. Accelerative time dilation is scale-upshift caused by kinematic overhead.

The clock law governing proper time is:

$$\frac{d\tau}{d\tau_0} = e^{-s_{\text{obs}}}$$

where s_{obs} is the observer depth at the system's location. Geometry, by contrast, responds to s_{geom}, the full-cycle depth (with $s_{\text{geom}} = 2\, s_{\text{obs}}$ in the linearised symmetric bipolar regime).

11.4 The Equivalence Principle in STT

The equivalence principle, the empirical fact that gravitational and accelerative time dilation are locally indistinguishable, follows directly:

Gravity and acceleration both act as scale-upshifts (shifts to higher effective scale), which produce Scale-Flux slowdown and therefore time dilation.

The causal chain is identical in both cases: scale-upshift → Scale-Flux slowdown → time dilation. The two phenomena are not merely analogous; they are the same mechanism operating through different triggers (render cost versus kinematic overhead). STT does not need to postulate equivalence separately, it emerges from a shared scale-upshift mechanism.

11.5 Connection to OSR

Scale-upshift does not only slow the clock. By shifting the system to higher effective scale, where Scale Flux is slower, it also increases local OSR. This means that time dilation and increased classical stability go hand in hand: regions of strong gravity are also regions of enhanced reconstruction stability. The gravitational field is simultaneously a clock-slowing field and a classicality-enhancing field, both arising from the same scale-upshift.

This feedback loop is the structural reason that gravity and quantum mechanics appear entangled in our observations, not because they need to be unified, but because they share a common origin in the scale-dependent rate of Scale Flux.

12 THE SCALE-RING LADDER: NAMED SCALES AND COSMIC EPOCHS

12.1 Cosmic History as a Scale-Ring Ladder

STT reframes cosmic history not as a timeline measured in years since a primordial explosion, but as a ladder of scale bands ordered by Scale Flux. "Epochs" are stability regimes, not calendar dates. Scale-Flux slowdown means each successive epoch is experienced as longer-lived and more stable than the last, a natural arrow of increasing classicality.

12.2 The Big Bang as a Boundary Outside Coordinate Time

Because coordinate time does not exist before the Master Sampler, the "Big Bang" in STT is not an event that occurred at some moment in the past. It is a boundary condition outside ordinary time: the rotating bipolar source, the yin-yang-like phase seed, that initiates the spectral carrier on the scale plane.

12.3 The Named Scale-Rings

STT identifies several named bands on the scale-ring ladder: the neutrino band at σ_1 (first-sampled, maximally aliased), the nuclear/pion band (where strong binding appears), the electron/atomic band (where EM-dominated stable atoms form), the molecular/chemical band, the biological band, the planetary/stellar band, and the galactic band. Each band is characterized by its OSR, its dominant interaction channels, and its stability profile.

13 THE OBSERVER AS NESTED SCALES: ROAM VERSUS ANCHOR

13.1 From Single Scale-Ring to Nested Stack

A physical observer, a human, a detector, a biological system, does not live at a single scale-ring. It spans a range of nested scale bands, from the atomic scale (where its chemistry operates) through the molecular and cellular scales to the macroscopic body scale. This nested range is the observer stack.

13.2 Anchor Bands: Storage and Execution

Within the observer stack, anchor bands are high-OSR, slow-scale-clock zones where reconstruction is most stable. These are the sites of memory, persistent storage, and reliable execution, the bands where patterns endure long enough to serve as records and computational substrates.

13.3 The Roam Band: Exploration and Novelty

The roam band is the alias-rich, faster-flux margin within the observer stack. It supports exploration, novelty, and candidate generation, patterns that are flexible, uncommitted, and open to rapid recombination.

13.4 The Roam-to-Anchor Cycle

Cognition, learning, and adaptation can be understood as a roam-to-anchor cycle: the roam band generates candidates (novel patterns, flexible associations), and successful candidates are promoted to anchor bands (stable memory, committed structure). The roam band is where Scale Flux is relatively faster, patterns remain flexible, and commitment has not yet occurred.

14 WHEEL KINEMATICS: STROBOSCOPIC ARTIFACTS OF SAMPLING

Discrete sampling of periodic patterns produces familiar stroboscopic illusions: a wheel filmed at certain frame rates can appear to spin slowly, stop, or rotate backward. The underlying rotation has not changed; only the sampling relationship has.

The same logic applies within the Master Sampler. When the sampler updates on discrete ticks, motion is represented modulo the repeating structure of the reconstructed lattice. Near wrap boundaries, especially close to the heavily aliased regime around σ_1, where Scale Flux is fast and OSR is low, apparent dynamics can look frozen or retrograde without any new force acting. This is purely a readout alias artifact, and it provides an intuitive bridge from the everyday stroboscopic effect to the "strange" kinematics of quantum mechanics in low-OSR regimes.

Quantum tunneling, barrier reflection, and zero-point oscillation can all be viewed through this lens: not as mysterious violations of classical logic, but as expected aliasing behavior of a discrete sampler operating near its representational edge.

15 FORCE EMERGENCE: SAMPLER STRUCTURE

In STT, forces are not independent theoretical sectors layered on top of spacetime. They emerge, in a definite structural order, from the sampler's own operational requirements. This is a direct consequence of the deeper-foundation thesis: if spacetime is reconstructed, then the rules governing transport, consistency, and cost within that reconstruction are what we observe as forces.

15.1 Photons and the Bridge Constant c_x

Photons are the sampler's native null-update transport mode: the default way phase information propagates across the reconstructed lattice. They are not added as particles; they exist automatically as soon as the Master Sampler does.

This transport is governed by a fundamental bridge constant c_*, which sets the sampler's intrinsic conversion ratio between spatial steps (cell-to-cell updates) and time ticks (the sampling cadence). At the foundational level, c_* is the sampler's internal conversion constant. In later calibration, it is identified with the observed invariant speed of light.

Under Fourier readout, photons are the simplest phase-carrying update mode, the baseline way Fourier phases propagate from cell to cell, tick by tick.

15.2 Electromagnetism: Neighbor-Scale Phase Transport

Electromagnetism is not a "field substance" inhabiting a single scale band. In STT, it is defined as $U(1)$ phase transport between neighboring scale slices, it lives on the links connecting one σ -slice to the next.

The sampler maintains a scale register: a slice label tied to alias and wrap structure. Adjacent slices must hand off phase consistently to keep reconstruction coherent. The degrees of freedom on those inter-slice links are electromagnetism. Because it lives on links, EM is edge-exclusive and neighbor-local: dominant couplings connect only a slice and its immediate neighbors.

Charge, in this picture, is the stable discrete label of how a persistent configuration transforms under this neighbor-scale phase transport, how it "winds" around the scale ring. This is fundamentally a phase-bookkeeping rule.

Electromagnetic link phases act dominantly on q_+-sector degrees of freedom. The q_- sector has its own internal phase rules, but they do not couple directly to q_+ EM.

15.3 Gravity: Render-Cost Latency, Scale-Upshift, and Emergent Geometry

Gravity is not introduced as spacetime curvature. It emerges when the sampler carries persistent captured structure that is costly to maintain.

Durable, coherent configurations (high-persistence readout knots) increase the sampler's computational render load. This load induces a scale-upshift, a shift to higher effective scale, which produces Scale-Flux slowdown and therefore: local clocks dilate (the scale clock runs slower), space cells enlarge (local rulers stretch as resolution coarsens), and local representable bandwidth narrows (the Nyquist margin tightens).

Light bends and slows in these regions the way it would in a medium with a spatially varying refractive index. Gravity, in STT, is the geometry of render-cost–induced scale-upshift.

Crucially, geometry is sourced by the full bipolar reconstruction burden $B = q_+ + q_-$. Both sectors contribute to the total render load. Gravity is sector-blind: it responds to the entire reconstruction cycle, not just the q_+-projected observable part. In the linearised symmetric bipolar regime, this is why the geometric depth s_{geom} is twice the observer depth s_{obs}.

The same scale-upshift that slows the clock also raises local OSR, shifting the system toward more classical, more deterministic behavior. This is why gravitational wells are not sites of quantum chaos, they are sites of enhanced classicality, because Scale-Flux slowdown and high OSR go together.

15.4 The Force Emergence Ladder

The three forces appear in a definite structural order, not a timeline in years, but a sequence of operational milestones:

1. At Master Sampler ignition (σ_0): photons appear immediately as native null-update transport, governed by c_*.
2. As scale-slice structure becomes active: electromagnetism appears as neighbor-scale, edge-exclusive $U(1)$ phase transport (the link rule) implemented within reconstruction.
3. As persistent captured structure accumulates: gravity appears as render-cost–induced scale-upshift, sourced by the full bipolar burden $B = q_+ + q_-$, reshaping the local scale clock and producing emergent geometry.

16 SCALE LENSING: GRAVITY AS OPTICS IN THE SCALE DIMENSION

16.1 Beyond Spatial Bending

General relativity describes gravity as the bending of spacetime: mass curves the geometry through which light and matter travel. STT recovers this, but adds a second, deeper effect. Because gravity is render-cost–induced scale-upshift, a massive object does not only bend trajectories in reconstructed space. It also bends access across the scale dimension σ, changing which scale bands can couple into an observer's 4D readout.

This is scale lensing: the claim that mass acts as a lens not only in space but in the scale coordinate.

16.2 The Mechanism in One Chain

Scale lensing is produced by the same causal chain that produces time dilation, extended by one step:

persistent captured structure → render load → scale-upshift → Scale-Flux slowdown + cross-σ coupling → scale lens

The scale-upshift that slows the local clock also deforms the geometry of the readout slice in the σ-direction. This deformation increases cross-σ coupling: scale bands that normally remain decoupled from the observer's stable 4D slice begin to contribute measurably to reconstruction.

Time dilation and scale lensing are therefore two faces of the same effect, scale-upshift under load. Where there is strong gravitational dilation, there is also strong scale lensing.

16.3 What Scale Lensing Does

A scale lens changes the observer's access to normally hidden scale bands in three related ways:

Visibility shift: Deeper bands that ordinarily remain decoupled can begin to leave measurable fingerprints in the observer band, not as direct spatial images, but as changes in timing, spectral content, or field behavior.

Resonance emphasis: The lens can favor certain resonant bands over others, altering which stable structures are easiest to form or detect locally.

Stability reshaping: Because the lens modifies local sampling conditions, it effectively reshapes the OSR landscape, moving the boundaries between quantum-heavy and classical-stable behavior in the affected region.

"Seeing hidden scales" does not mean taking a direct picture of deeper-scale physics. It means enhanced coupling and imprint: signatures of normally inaccessible bands appearing as shifts in timing, dominant resonances, particle or field leakage, and spectral anomalies within the observer's accessible readout.

16.4 Lens Depth: A Compact-Object Taxonomy

Because scale lensing strength increases with persistent captured load, compact astrophysical objects form a natural ladder of lens depth, how deep a synthesis band can imprint into accessible readout. The lens-depth parameter is defined in terms of the full-cycle geometric depth:

$$\mathscr{L} = \frac{s_{\text{geom}}}{s_{\text{crit}}}$$

because deep lensing is about total geometric sourcing, the full bipolar reconstruction burden, not just the q_+-projected observable clock. The observed proper-time response is tied separately to s_{obs}.

The taxonomy:

L1, Neutrino Lens: Near-threshold coupling dominates. The maximally aliased first-sampled sector (σ_1) is emphasized. Minimal scale-upshift.

L2, Nuclear Lens: Strong enough to pull the nuclear/point synthesis band into accessible imprint. Hypothesis: the Sun-like stellar regime, where nuclear binding is the dominant energy source and nuclear-scale physics leaves clear spectral fingerprints.

L3, Electron Lens: Strong enough that electron-scale bands imprint robustly. The electron-degenerate regime, white-dwarf–like objects, where electron degeneracy pressure is the dominant structural feature.

L4, Neutron Lens: Extreme lensing where neutron-scale bands imprint dominantly. The neutron-star regime, where matter is compressed to nuclear density and neutron-scale physics governs structure.

L5, Render-Horizon Lens: Maximal scale-upshift creates an effective readout horizon: the boundary beyond which the outside observer's reconstruction process can no longer stably reconstruct interior dynamics. This is the black hole regime.

This classification restates the standard compact-object sequence as a scale-optics ladder: more persistent load → deeper scale lens → deeper synthesis bands become accessible, until reconstruction itself fails at the render horizon.

16.5 Pulsars as Scale-Lensing Beacons

A pulsar is naturally described as an L4 Neutron Lens with exceptionally coherent rotation: a stable, phase-locked, high-persistence object whose periodic emission functions as a clean stroboscopic beacon. In STT terms, pulsars are significant because they combine extreme scale-upshift (strong dilation), deep scale lensing (enhanced cross-σ coupling), and extraordinarily stable periodicity (a sensitive probe of sampler dynamics).

16.6 Black Holes as the Extreme: The Readout Horizon

In STT, a black hole is not a separate ontological category. It is the extreme limit of the same scale-lensing mechanism: render load drives an enormous scale-upshift. The full-cycle geometric depth s_{geom} approaches the critical threshold. As it does, the observable clock rate $d\tau/d\tau_0 = e^{-s_{\text{obs}}}$ approaches zero from the outside observer's perspective, the system is reconstructed ever more slowly until, at the readout horizon, stable access ceases entirely. Beyond the readout horizon, the outside observer's reconstruction can no longer maintain stable access to interior dynamics. The boundary is not a spatial wall, it is a reconstruction limit.

Binary spinning black-hole systems may represent the strongest visible 4D echo of the underlying bipolar reconstruction cycle, the closest reconstructed analogue of the deeper two-phase sourcing architecture that operates at the foundation of the theory.

17 SAMPLER EVOLUTION, EPOCH-DEPENDENT C_x, AND REDSHIFT

17.1 The Master Sampler Evolves with Scale Flux

The Master Sampler is not static. As the carrier continues to propagate outward and new scale bands become active, the sampler's operational parameters can evolve. This evolution is constrained, it must preserve consistency and the closure limit, but it is not frozen.

17.2 Two Evolution Modes: Drift and Scale-Leaps

Scale drift: Smooth, gradual evolution of the sampler's reconstruction parameters along Scale Flux. Continuously reshapes stability basins and accessible form-space.

Scale-leaps: Discrete sampler reconfiguration at a stability boundary between Scale-Harmonic basins. Opens new phase-lock basins; can produce saltational evolutionary jumps.

17.3 Cosmic Redshift as Epoch Mismatch

A photon emitted in one epoch and received in another carries the imprint of the earlier sampler state. If the bridge constant $c_*(\sigma)$ has drifted, the photon's encoded frequency no longer matches the receiver's current reconstruction parameters. The result is a frequency shift: cosmic redshift as epoch mismatch.

17.4 Unifying Cosmic, Gravitational, and Accelerative Redshift

STT unifies all three redshift types under one umbrella: metric mismatch between emitter and receiver. Cosmic redshift arises from drift in $c_*(\sigma)$ across epochs. Gravitational redshift arises from different s_{geom} at emitter and receiver, the same metric-based clock law that governs time dilation (Section 11) also governs the frequency shift. Accelerative redshift arises from kinematic-overhead differences in effective s_{geom}.

All three are instances of the same structural phenomenon: emission encoded under one effective metric, reception decoded under another. The observable frequency shift is always determined by the ratio of proper-time rates, not by raw OSR ratios, which track reconstruction stability rather than clock rates. The mathematical realization of this unification is given in Part 2 §43.

17.5 Sampler Evolution and the Stability Landscape

If the sampler evolves with $c_*(\sigma)$, then the stability map evolves too: which bands carry high OSR, which Scale-Harmonic Rings are strong attractors, which persistent knots and composites can stably exist. "Evolution" in the broadest STT sense is the progressive opening and clos-

ing of stability basins as the sampler matures along Scale Flux, enabling richer, longer-lived structure at deeper scale epochs.

This connects directly to scale lensing: massive objects induce scale-upshift and enhance cross-σ coupling, increasing the degree to which hidden epochs and their stability signatures can imprint on observable readout. The lens-depth taxonomy (L1–L5) classifies how deep this epoch-bridging access extends.

17.6 A Discipline Constraint

Any epoch dependence in c_* must ultimately be expressed through drift in dimensionless observable ratios, not as "a changing speed" in isolation. The bridge constant is the sampler's internal conversion; what observers can measure are ratios of physical quantities that shift when that conversion changes. This constraint ensures that claims about epoch-dependent c_* are operationally meaningful and empirically testable.

18 SCALE-DRIVEN EVOLUTION IN FOUR DIMENSIONS

The sampler evolution described in the previous section has direct consequences for biological evolution as observed in our 4D slice. Scale drift and scale-leaps do not replace genetics, natural selection, or ecology. They reshape the stability landscape within which those mechanisms operate, determining what kinds of structures can persist, what coordination modules are available, and how fast viable novelty can accumulate.

18.1 Scale Drift: The Moving Envelope Behind Ordinary Evolution

During scale drift, the Master Sampler evolves slowly along Scale Flux, continuously reshaping the conditions under which biological structure must persist. In practical terms, drift shows up as: a gradual change in OSR conditions and phase-lock basins, altering which configurations are robustly stable; a gradual change in cross-scale coupling, altering what can reliably coordinate across the nested organism stack; a gradual change in accessible form-space, the set of biological architectures that can persist as stable readout knots under current sampler conditions; and a gradual change in innovation rate, how often viable novelties survive long enough to become selectable.

Scale drift = slow reshaping of what can stably exist; evolution is selection exploring that moving envelope.

18.2 Scale-Leaps: New Stable Possibilities Without Visible Intermediates

Scale-leaps are not "faster drift." They are qualitatively different: discrete reconfigurations of the sampler at a stability boundary. When a scale-leap opens a new phase-lock basin, entirely new kinds of stable structure become available at once, not by gradual refinement of existing structures, but by the sudden availability of a previously inaccessible stability regime.

This naturally produces the pattern paleontologists call saltation or punctuated equilibrium: long periods of stability (the sampler in a settled basin) interrupted by rapid bursts of new form (the sampler crossing a stability boundary and opening new basins).

18.3 Cambrian-Type Bursts

The Cambrian explosion, the sudden appearance of most major animal phyla in a geologically short window, is naturally explained as a scale-leap event: the Master Sampler crossed a stability boundary that opened new phase-lock basins corresponding to new body-plan architectures. The "explosion" was not a failure of gradualism; it was the expected outcome of a sampler reconfiguration that made new forms stably representable.

18.4 Connection to the Roam-Anchor Architecture

Scale-leaps interact with the observer stack's roam-anchor structure. A scale-leap that reconfigures the roam band (the alias-rich margin where novelty is generated) changes the menu of candidate patterns; a scale-leap that touches the anchor bands (where committed memory and execution live) can destabilize or reorganize existing architecture. The interplay between roam-band candidate generation and anchor-band commitment under evolving sampler conditions provides a rich but principled account of evolutionary dynamics.

19 PARTICLE ONTOLOGY: STABLE READOUT KNOTS

Particles in STT are not fundamental point objects inhabiting a pre-existing spacetime. They are **stable readout knots**: persistent, localized configurations of reconstructed phase structure that survive across many ticks in phase-lock basins.

A readout knot forms when a particular pattern of stored spectral content, amplitudes and phases distributed across Fourier bins, becomes self-reinforcing under the sampler's tick-by-tick update. The pattern reconstructs itself each cycle, not because it is imposed from outside, but because its internal phase relationships are harmonically aligned with the sampler's reconstruction architecture. It sits in a basin of stability: small perturbations are absorbed rather than amplified, and the configuration persists.

What determines whether a knot is stable is the same OSR-dependent architecture that governs all reconstruction. A knot persists where alias residuals are low and harmonic alignment is favorable, where the sampler's resolution is sufficient to faithfully reproduce the pattern tick after tick. At low OSR, near the representational edge, knots are fragile: alias agitation can disrupt the phase relationships that hold them together, and patterns dissolve or transform rapidly. At high OSR, deep in the classical regime, knots are robust: the reconstruction margin is wide, perturbations decay, and patterns endure across enormous numbers of ticks.

Mass, in this picture, is render cost. A readout knot that requires the sampler to maintain more persistent captured structure, more spectral content held in coherent phase-lock, imposes a greater render burden on the local reconstruction. That burden produces scale-upshift, which produces time dilation and gravitational coupling. Heavier particles are costlier knots.

Charge is phase-winding structure. A knot's discrete label under the neighbor-scale $U(1)$ phase transport, how it transforms when the sampler applies its inter-slice bookkeeping, is its charge. This is not an additional property attached to the knot; it is part of the knot's internal phase architecture, determined by how the stored spectral content winds around the compact scale-phase coordinate θ.

Spin and internal quantum numbers arise from the knot's transformation properties under the sampler's closure algebra, the 8-dimensional real closure space of §37.1 in Part 2. The octonionic closure limit caps the number of independent internal directions, which is why the particle zoo is finite and structured rather than unbounded. The specific mapping from closure directions and winding modes to observed particle families, masses, and mixing angles is completion-layer work.

What STT changes about particle ontology is the direction of explanation. In standard physics, particles are fundamental and spacetime is their stage. In STT, the reconstruction is fundamental and particles are the patterns it can stably maintain, knots in the readout that persist be-

cause the sampler's architecture favors them. A particle exists not because it was placed into spacetime, but because the sampler's phase-lock landscape has a basin at that configuration.

20 SCALE COHERENCE AND THE RENDER STRESS TENSOR

20.1 Scale Coherence: Consistency Across the Scale Dimension

The sampler does not operate at a single scale; it reconstructs across a continuum of σ-slices. For this reconstruction to be consistent, for the 4D readout to be a stable, self-consistent physical world, neighboring scale slices must remain mutually consistent. This is scale coherence: the requirement that each slice remain self-consistent while absorbing information from smaller scales.

20.2 Why a Scalar Is Not Enough

A single number per point cannot track the full complexity of reconstruction: burden can flow in different directions, accumulate differently under different conditions, and convert between persistent captured structure and transient alias churn. Describing this requires a tensor.

20.3 The Render Stress Tensor: What It Tracks

The render stress tensor is the bookkeeping object that encodes: render burden density (the amount of coherent structure the sampler maintains in a region), spatial burden current (where that maintained structure is moving in reconstructed space), scale transport current (flow of coherent burden along σ), and directional stresses (pressure, shear, the anisotropic cost structure of maintaining coherence).

20.4 The Scale Coherence Rule: Conservation Generalized to Include σ

Scale coherence imposes a conservation rule: a region can only gain or lose coherent burden via currents (spatial or scale) or conversion between churn and persistent capture. Burden cannot appear or vanish without accounting. This is the STT analogue of local conservation, generalized to include the scale dimension σ.

20.5 OSR Inside the Tensor Picture: Laminar versus Turbulent

OSR determines the character of the tensor's dynamics. At high OSR, coherence transport is smooth, perturbations decay, and the tensor behaves classically (laminar readout). At low OSR, alias agitation dominates, perturbations amplify, and the tensor behaves stochastically (turbulent readout).

20.6 What This Enables (Without Committing to Specific Equations)

The render stress tensor provides the scaffolding needed to write genuine field dynamics, equations that govern how render burden evolves, flows, and sources geometry. Part 2 formalizes this scaffolding.

20.7 Render Burden Density and Burden Currents

The tensor's temporal diagonal component is the render burden density ρ_R, the inventory of coherent structure at a given point and scale. The mixed temporal-spatial components are burden currents J^i and the temporal-scale component is the scale transport current J^σ.

20.8 Continuity of Coherence

The conservation rule takes the form of a continuity equation generalized to $3 + 1 + \sigma$: the rate of change of burden density plus the divergence of spatial currents plus the σ-derivative of scale transport equals zero (up to conversion between captured and churn components).

21 DRAG, VISCOSITY, AND FLOW REGIMES IN A FILTERLESS SAMPLER

21.1 Why Drag Appears

In a filterless sampler, maintaining coherent readout under changing conditions is not free. When the sampler must reconcile rapidly changing alias patterns, transport coherent burden across scale slices, or maintain stability near the representational edge, the reconstruction develops backpressure, an effective drag.

21.2 OSR as the Viscosity Dial

OSR governs how easily coherence flows through the reconstructed lattice. High OSR: smooth flow, low effective viscosity, classical transport. Low OSR: rough flow, high effective viscosity, quantum-heavy transport with alias-driven turbulence.

21.3 Laminar versus Turbulent Readout

This is a concrete realization of the two-regime picture: laminar readout (classical, predictable, smooth) at high OSR, turbulent readout (quantum-heavy, stochastic, interference-rich) at low OSR. The transition is not sharp but continuous, governed by the local OSR gradient.

21.4 Drag in the Render Stress Picture

Drag manifests in the render stress tensor as off-diagonal stress components and as non-trivial scale transport. It is the observable signature of coherence cost in a filterless sampler, stress backreaction from maintaining scale coherence near the aliasing edge.

21.5 When Motion Outruns Sampling

At very low OSR, systems can change faster than the sampler can stably reconstruct them. The result is maximal alias ambiguity, the quantum-mechanical limit where outcomes are genuinely probabilistic and interference effects are dominant.

21.6 Galaxy versus Solar System: Different Flow Regimes at Different σ

The flow-regime picture maps directly onto the dark-matter discussion. A solar system, with lower system coordination index σ_{sys} and lower coordination cost, operates in a more laminar flow regime overall. A galaxy, with higher σ_{sys} and massive coordination cost, operates in a regime where scale transport, drag, and nonlinear render response become significant, producing the stronger effective gravitational response that is interpreted as dark matter. Within a galaxy, the local stability margin $\text{OSR}_{\text{local}}(r)$ can vary from high (in dense inner regions) to low

(in sparse outskirts), so the flow character is position-dependent even within a single high-σ_{sys} system.

22 THE BOHR RADIUS: FIRST QUANTITATIVE CONTACT

22.1 The Starting Point: What a Filterless Sampler Cannot Do

A filterless sampler cannot produce arbitrarily sharp features: there is a minimum resolvable length, set by the lattice spacing. Stable atomic structure must respect this limit.

22.2 Linking OSR to the Fine-Structure Constant via a Velocity Ratio

At the hydrogen scale-ring, the OSR calibration hypothesis gives $\mathrm{OSR}_H \sim 1/\alpha \approx 137$. The fine-structure constant α measures the fractional alias residue at the first fully stable atomic band.

22.3 The Bohr Radius as Compton Length Times OSR

Let the electron base length be identified with the reduced Compton wavelength $\bar{\lambda}_e = \hbar/(m_e c)$. Then OSR inflation yields the hydrogen length scale:

$$a_0 \;=\; \frac{1}{\alpha}\,\bar{\lambda}_e \;=\; \frac{\hbar}{m_e\, c\, \alpha}$$

The Bohr radius is the Compton length inflated by the oversampling safety factor. The atom is as large as the sampler's stability margin allows.

22.4 What the Fine-Structure Constant Means in STT

In STT, α is the sampler's fractional alias residue at the hydrogen band, the fraction of the null-transport speed c_* that appears as residual non-phase-locked drift. At the hydrogen scale-ring, the reconstruction is stable enough to support persistent atomic structure, but a small fraction of the sampler's null-transport capacity survives as residual alias drift rather than being locked into stable phase structure. That fraction is $\alpha \approx 1/137$. The fine-structure constant is therefore not a fundamental constant in the usual sense; it is a derived characteristic of a particular scale band, measuring how close the hydrogen band is to perfect phase-lock. This interpretation, that α is the sampler's leftover alias agitation at the first stable atomic scale, is one of the theory's most evocative and potentially testable contact points with known physics.

22.5 Clean Readout: An Operational Definition

Clean readout is the operational condition where alias backreaction is dynamically negligible. Achieved when OSR is everywhere above a stability threshold (approximately $1/\alpha$ at the hydrogen band).

22.6 Status and Scope

This calibration sketch is a contact point, not a full prediction. It shows that STT's framework, when calibrated at the hydrogen scale, reproduces the correct atomic length scale. Extending this to heavier atoms, molecules, and multi-body systems is completion-layer work.

23 THE KALUZA–KLEIN PHASE-FIBER VIEW

23.1 The Full STT Coordinate Structure

The post-MSS framework involves two distinct extra-coordinate structures beyond the four reconstructed spacetime dimensions:

The **render index** σ is noncompact and monotone. It orders the scale-ring ladder, carries $\mathrm{OSR}(\sigma) \propto e^{2\sigma}$, supports epoch structure, and governs the scale clock. The global STT architecture is $3 + 1 + \sigma$.

The **scale-phase angle** $\theta \in [0, 2\pi)$ is a compact internal coordinate at each σ-slice, parameterising the $U(1)$ neighbor-scale bookkeeping that STT identifies as electromagnetism. The KK construction operates on the local phase-fiber package (x^μ, y) with $y = R\theta$ at each σ-slice.

These are different objects. The KK reformulation is a local phase-fiber model at each σ-slice, not a compactification of the global render index and not an additional global spacetime dimension. The global STT effective arena is $3 + 1 + \sigma$; the compact phase fiber θ is attached locally at each slice, in the manner of a fiber bundle. The KK view is a local effective description useful for understanding electromagnetism and charge quantization; it is not a claim about the global topology or dimensionality of the underlying pre-geometric substrate.

23.2 Scale Slices as Preferred 4D Bands

Within the global $3 + 1 + \sigma$ structure, each σ-slice is a preferred 4D band, a specific scale depth with its own OSR, scale clock, and reconstruction conditions. The KK phase fiber θ sits at each such slice, encoding inter-slice phase consistency.

23.3 Electromagnetism as Geometry of the Phase Fiber

In the Kaluza–Klein reformulation, the $U(1)$ phase transport that STT identifies as electromagnetism emerges as the geometric connection of the compact scale-phase coordinate θ, the standard KK mechanism. The compact coordinate is the internal phase at each σ-slice, not the render index σ itself.

23.4 Charge Quantization as Phase-Winding Number

Charge in the KK picture is the mode number of a field's winding around the compact scale-phase coordinate θ. Positive and negative charges correspond to opposite winding orientations.

23.5 Gravity and the Scale-Upshift Field

The scale-upshift field $s(x)$, now understood as split into s_{geom} and s_{obs}, maps to the KK radion/dilaton scalar within the local phase-fiber model. Gravity emerges from the local phase-fiber geometry in the standard KK way, with the sector split ensuring that the geometric field (dilaton) and the clock response (observed proper time) maintain their distinct roles. The global σ-dependence of gravity (epoch structure, scale-clock running, OSR scaling) lives in the non-compact render index, not in the compact KK fiber.

23.6 Why the Phase-Fiber View Is Useful

The local KK reformulation provides a compact mathematical home for electromagnetism, charge quantization, and the dilaton/gravity coupling at each σ-slice. The render stress tensor, scale lensing, and epoch-dependent structure live in the full $3 + 1 + \sigma$ framework. The two coordinate structures are complementary: σ handles the global scale architecture, θ handles the local $U(1)$ phase geometry.

24 SUMMARY

Scale-Time Theory proposes that quantum mechanics and general relativity are not two theories awaiting unification but two faces of a single, deeper system, a spectral carrier on a pre-geometric scale plane.

A carrier propagating outward in scale under constant throughput from a rotating bipolar source generates a truncated bipolar Fermat sweep whose cumulative spectral burden grows as ρ^2. Scale Flux, the rate of this outward propagation, decelerates with increasing scale depth. When the cumulative burden at the ignition ring exceeds the threshold for continuous readout, a Master Sampler ignites at σ_0, a scale-ring sampler whose input is the regularized angular trace of the carrier approaching that ring from inside, introducing discrete time, reconstructed space, and Fourier readout. The first sampled band (σ_1, the Nyquist–Shannon scale-ring) is maximally aliased, a candidate for the neutrino sector.

Scale-Flux slowdown directly generates the oversampling ratio: fast flux yields low OSR and quantum behavior; slow flux yields high OSR and classical stability. Classical reality anchors on Scale-Harmonic Rings where harmonic alignment and slow flux cooperate to suppress alias ambiguity.

The sampler's internal bookkeeping closes on an octonionic eight-direction basis, capping the number of independent internal channels. This closure naturally supports a full bipolar reconstruction cycle (q_+, q_-), the post-MSS continuation of the pre-geometric dipole source, where the q_+ sector defines our electromagnetically visible world and the q_- sector hosts a counter-phase channel with suppressed EM visibility. Dark-matter phenomenology is decomposed into two layers: a universal hidden co-burden from the full bipolar cycle (the q_- sector contributes gravitating burden that is not directly visible in q_+ electromagnetic observation), and a scale-dependent enhancement from scale-clock running (systems at higher render index operate on a slower scale clock, amplifying the effective gravitational response). The combination of hidden co-burden and scale-clock enhancement explains why geometry exceeds visible matter universally, and why the excess strengthens in high-σ systems such as galaxies and clusters.

The geometric field is sourced by the full bipolar reconstruction cycle. Observable proper time is measured only in the q_+-projected readout sector, which counts one effective phase per full cycle. In the linearised symmetric bipolar regime, this sector-clock architecture conditionally yields two distinct depths: the geometric depth s_{geom} that shapes spacetime, and the observer depth $s_{\mathrm{obs}} = s_{\mathrm{geom}}/2$ that governs clocked observables. Geometry therefore responds to the full reconstruction burden, while clocked observables register only the visible half-cycle.

Observable time is set by the scale clock, the local Scale-Flux rate. Time dilation, whether gravitational or accelerative, follows a single causal chain: scale-upshift → Scale-Flux slowdown →

time dilation. The equivalence principle is not postulated separately; it emerges structurally from the shared scale-upshift mechanism.

Forces arise as sampler structure: photons as native transport governed by c_*, electromagnetism as neighbor-scale $U(1)$ phase bookkeeping, and gravity as render-cost–induced scale-upshift sourced by the full bipolar burden $B = q_+ + q_-$, producing emergent geometry. The same scale-upshift that produces time dilation also produces scale lensing, bending access across the scale dimension so that deeper synthesis bands can imprint on the observer's readout, with compact objects forming a natural lens-depth ladder from neutrino coupling to the render horizon.

To move beyond static descriptions, STT introduces a render stress tensor that tracks render burden density, spatial flow, directional stresses, and coherence transport along the scale dimension σ. Scale coherence is the closure rule: burden can move through space, move along σ, and convert between alias churn and persistent captured structure, but every change must be accountable.

25 GLOSSARY PART 1

Accessible form-space. The set of biological architectures that can persist as stable readout knots under current sampler conditions. Reshaped by scale drift and scale-leaps.

Anchor bands. High-OSR, slow-scale-clock zones within the observer stack. Sites of memory, storage, and execution.

Bipolar reconstruction cycle, full. The complete two-phase sourcing cycle of the sampler, involving both q_+ and q_-. The post-MSS continuation of the pre-geometric dipole source. The geometric field is sourced by this full cycle.

Bohr radius (STT derivation). The electron's Compton-like base length multiplied by the hydrogen OSR ($1/\alpha$). The atom is as large as the sampler's stability margin allows.

Bridge constant c_*. The sampler's intrinsic conversion ratio between spatial steps and time ticks. Governs photon transport speed.

Clean readout. Operational condition where alias backreaction is dynamically negligible. Achieved when OSR is everywhere above a stability threshold (approximately $1/\alpha$ at the hydrogen band).

Coherence boundary. The interaction boundary a system presents to the sampler, the extent of mutual coupling that must be reconciled per update. Not literal geometric area.

Continuity of coherence. The conservation rule: a region can only gain or lose coherent burden via currents (spatial or scale) or conversion between churn and persistent capture.

Counter-phase sector (q_-). The q_- reconstruction channel. Antimatter-like partner sector defined by the bipolar reconstruction cycle. Contributes hidden co-burden to the total geometric source (Layer 1 of dark-matter decomposition). Not identical to laboratory antimatter; EM-suppressed in q_+ readout.

Cumulative spectral burden $C_H(\rho)$. The total spectral inventory inscribed in the carrier up to radius ρ. Grows as $\chi_H\,\rho^2$ (equivalently $\chi_H\,e^{2\sigma}$), where the source-shape factor χ_H depends on the architecturally fixed bipolar profile. The ρ^2 scaling is universal; χ_H sets only the prefactor. The correct monotone crowding variable that triggers MSS ignition when it reaches the representability threshold C_{crit}.

Dark matter (STT). Decomposed into two layers: (1) a universal hidden co-burden from the full bipolar reconstruction cycle, the q_- sector contributes gravitating burden not visible in q_+ electromagnetic observation; and (2) a scale-dependent enhancement from scale-clock running, higher-σ systems produce stronger effective gravitational response. The combination ex-

plains why geometry exceeds visible matter universally and why the excess strengthens in galaxies and clusters. Not a new substance.

Dipole source. The rotating bipolar seed at the puncture of the scale plane. Formally a puncture-centered bipolar drive (Axiom A2); intuitively visualized as a yin-yang-like rotating double core, a coherent two-lobed phase exciter whose opposite lobes remain phase-linked while the whole pattern rotates (the formal theory works in the zero-core limit of this picture). In signal-processing terms: a balanced rotating phase transmitter writing a structured angular waveform into an outward transport channel; the MSS is the first ring receiver where that waveform must be discretely sampled. Generates a truncated bipolar Fermat sweep. The pre-geometric ancestor of the post-MSS full bipolar reconstruction cycle.

Drag (STT). Not an added force. The observable signature of coherence cost in a filterless sampler, stress backreaction from maintaining scale coherence near the aliasing edge.

Electromagnetism. Neighbor-scale, edge-exclusive $U(1)$ phase transport implemented in reconstruction bookkeeping.

Effective gravitational response. The combined gravitational effect of hidden co-burden and scale-clock enhancement: $M_{\text{eff}} \sim (M_{q_+} + M_{q_-})\,\Xi_\sigma$. What an observer infers as "gravitating mass" from dynamics or lensing.

Epoch-dependent $c_*(\sigma)$. The bridge constant as a function of scale epoch. Slice-local but can vary across σ-epochs via scale drift or scale-leaps.

Epoch-mismatch redshift. Frequency shift caused by decoding a photon under a different effective metric than the one under which it was emitted. Determined by the ratio of proper-time rates (metric-based), not by OSR ratios. Unifies cosmic, gravitational, and accelerative redshift.

KK phase-fiber view. Local effective Kaluza–Klein model at each σ-slice, operating on the compact scale-phase coordinate $\theta \in S^1$ with $y = R\theta$. EM and charge from the compact phase geometry; gravity coupling via the dilaton. Not a compactification of the global render index σ and not an additional global spacetime dimension. The global STT arena is $3 + 1 + \sigma$; the KK phase fiber θ is attached locally at each slice.

Fourier readout. Inverse synthesis procedure that converts the stored (alias-summed) bin content, originally seeded from ring-trace angular projection and lift, into reconstructed physical field patterns across the lattice each tick.

Frequency ramp (cumulative spectral burden). The growing spectral inventory caused by steady bipolar rotation being written into an outward-propagating carrier. Not a local-wavenumber effect (the local phase gradient decreases outward), but a cumulative-inventory

effect: spectral burden grows as $\chi_H\,\rho^2$, with the ρ^2 scaling universal and the prefactor set by the fixed source profile. The mathematical content is Theorem T1 (§30.2).

Geometric depth $s_{\mathrm{geom}}(x)$. The full-cycle scale-upshift field sourcing geometry, gravity, and lensing. Responds to the total bipolar burden $B = q_+ + q_-$. In the linearised symmetric bipolar regime, related to observer depth by $s_{\mathrm{geom}} = 2\,s_{\mathrm{obs}}$ (C7).

Gravity. Scale-upshift induced by render cost of persistent structure → emergent geometry; slows the scale clock and shifts local OSR. Sourced by the full bipolar burden.

Hidden co-burden. The gravitating burden contributed by the q_- sector of the full bipolar reconstruction cycle. Not directly visible in q_+ electromagnetic observation, but gravitationally active. Provides a universal baseline of "excess" geometry relative to visible matter alone. The first layer of STT's dark-matter decomposition.

Innovation rate. The rate at which viable biological novelties can stabilize long enough to become selectable. Governed by current OSR and phase-lock conditions.

Laminar readout. High-OSR regime where coherence transport is smooth, perturbations decay, and dynamics are classical and predictable.

Lens depth (L1–L5). Classification of compact objects by how deep a synthesis band can imprint into accessible readout, from neutrino lens (L1) to render-horizon lens (L5). Defined in terms of $s_{\mathrm{geom}}/s_{\mathrm{crit}}$.

Local stability margin $\mathrm{OSR}_{\mathrm{local}}(r)$. The oversampling ratio at a specific position within a system. Can be low even in high-σ_{sys} systems (e.g., galaxy outskirts). Distinct from the system coordination index: σ_{sys} characterises the system globally, $\mathrm{OSR}_{\mathrm{local}}$ varies with position.

Master Sampler. Scale-ring sampler igniting at the critical ring σ_0 (coordinate value $\sigma_0 \equiv 0$ under the normalization $\sigma = \ln(\rho/\rho_0)$). Not a filled region or a transformation of the whole scale plane; its ignition locus is the ring at ρ_0 and its sole input is the regularized angular trace of the carrier approaching that ring from inside ($\rho \to \rho_0^-$). Takes the ring-trace arrival signal at each tick, decomposes it by angular projection into coefficients, lifts these via the lift map into a pre-alias spectrum, alias-sums into stored bins, and produces physical space by inverse Fourier synthesis on the reconstructed lattice. Defines ticks, cells, bins, and readout.

Octonionic closure limit. Stability postulate: the sampler's internal bookkeeping closes on an eight-direction basis, capping the number of independent internal channels.

Observer depth $s_{\mathrm{obs}}(x)$. The projected-sector scale-upshift governing measured clock slowdown. Counts one effective phase per full bipolar cycle. In the linearised symmetric bipolar regime, related to geometric depth by $s_{\mathrm{obs}} = s_{\mathrm{geom}}/2$(C7).

Observer stack. Nested scale bands from pion/observer band to body scale supporting a physical observer.

OSR (oversampling ratio). The margin between the MSS clock and a system's own clock. High OSR = many samples per meaningful change = classical; low OSR = under-resolved = quantum.

OSR calibration hypothesis. At the hydrogen scale-ring, OSR $\sim 1/\alpha \approx 137$. The fine-structure constant measures the fractional alias residue at the first fully stable atomic band.

q_+-projected observer sector. The readout channel from which observable proper time and electromagnetically visible physics are measured. Registers one effective phase per full bipolar cycle.

Readout horizon. The boundary beyond which an outside observer's reconstruction process can no longer access interior dynamics. The STT description of a black hole boundary.

Readout knots. Stable, localized particle-like configurations persisting across many ticks in phase-lock basins.

Render burden density. The amount of coherent structure the sampler maintains in a region. The "inventory" component of the render stress tensor.

Render Capacity Postulate. Each σ-slice has a fixed total render capacity per cycle, a bounded amount of coherent updating per slice, per tick. The post-MSS operational form of the Scale-Flux Velocity Law.

Render stress tensor. Bookkeeping object tracking render burden density, spatial flow, directional stresses (pressure/shear), and coherence transport along σ. The source structure for Part 2's field equations.

Roam band. Alias-rich, faster-flux margin within the observer stack. Supports exploration, novelty, and candidate generation.

Scale clock. The local Scale-Flux rate that sets the system's time rate in post-MSS readout. Proper time is a readout of the scale clock, measured in the q_+-projected sector.

Scale-clock enhancement (Ξ_σ). The scale-dependent amplification factor by which the effective gravitational response increases in higher-σ systems. Near unity for low-σ systems (solar systems); significantly larger for high-σ systems (galaxies, clusters). The second layer of STT's dark-matter decomposition.

Scale-clock running. The dependence of effective gravitational response on the local scale clock. Large-scale bands (slower clock) produce stronger curvature per unit baryonic load than small-scale bands (faster clock). The mechanism underlying scale-clock enhancement.

Scale coherence. The consistency law requiring each scale slice to remain self-consistent while absorbing information from smaller scales. The STT analogue of local conservation, generalized to include σ.

Scale drift. Smooth, gradual evolution of the sampler's reconstruction parameters along Scale Flux. Continuously reshapes stability basins and accessible form-space.

Scale Flux. Directed outward propagation from small to large scale depth. Decelerates with increasing scale. The primary "arrow" ordering the scale-ring ladder.

Scale-Flux slowdown. The deceleration of Scale Flux with increasing scale depth, governed by the Scale-Flux Velocity Law. The single primitive from which OSR and the scale clock are derived.

Scale-Flux Velocity Law. Named principle: the effective rate of Scale Flux decreases with increasing render index because each σ-slice has fixed render capacity and larger-scale coherence boundaries require more processing.

Scale-Harmonic Rings. Stable phase-lock bands where alias residuals collapse to near-DC. Classical anchors reinforced by Scale-Flux slowdown.

Scale-leap. Discrete sampler reconfiguration at a stability boundary between Scale-Harmonic basins. Opens new phase-lock basins; can produce saltational evolutionary jumps.

Scale lensing. The bending of access across the scale dimension by mass. A direct consequence of scale-upshift: deeper synthesis bands gain enhanced coupling into the observer's 4D readout.

Scale-shift. A change in a system's effective scale involvement (up or down). The umbrella term for scale-upshift and scale-downshift.

Scale-upshift. A scale-shift toward higher effective scale, typically caused by render load or acceleration. Produces Scale-Flux slowdown and time dilation.

Sector-Clock Principle. The geometric field is sourced by the full bipolar reconstruction cycle (q_+, q_-), while observable proper time is measured in the q_+-projected readout sector and therefore counts one effective phase per cycle. The specific factor-of-two ($s_{\text{geom}} = 2\, s_{\text{obs}}$) is conditionally derived in the linearised symmetric bipolar regime from four assumptions: bipolar equipartition (A13), stationary burden symmetry (P6), the observer source law (C7-ii), and shared linearised coupling (C7-iii). See Conditional Result C7.

Bipolar equipartition (A13). The two sectors of the bipolar cycle have equal closure capacity: $\dim(P_{q_+}\mathscr{R}) = \dim(P_{q_-}\mathscr{R}) = 4$ in the 8-dimensional real closure space.

Stationary burden symmetry (P6, local form). For stationary configurations that do not spontaneously break bipolar symmetry, the local render burden densities in the two sectors are equal at each point: $b_{q_+}(x) = b_{q_-}(x)$ for all x. The integrated burdens $B_{q_\pm}$ inherit this equality.

Conditional Result C7. Given A13, P6, the observer source law (C7-ii), and shared linearised coupling (C7-iii), the geometric depth is twice the observer depth: $s_{\text{geom}} = 2\, s_{\text{obs}}$. The factor-of-two is a conditional consequence of the symmetric bipolar architecture plus the assumption that both depth fields respond to their respective sector burdens through the same linearised operator.

Spatial burden current. Flow of maintained coherent burden across the reconstructed 4D slice. Transport of outcomes through physical space.

Scale transport current. Flow of coherent burden along σ, the promotion of smaller-scale detail into larger-scale outcomes and the feedback when higher-scale constraints compress smaller scales.

σ (scale dimension / render index). Post-MSS fifth coordinate measuring render burden. Noncompact and monotone. Higher σ means higher render cost, slower scale clock, higher OSR on stable bands, and stronger effective gravitational response.

σ_{sys} (system coordination index). The global render index of a system as a collective structure, determined by its total coordination surface. Drives scale-clock enhancement Ξ_σ. Distinct from the local stability margin $\text{OSR}_{\text{local}}(r)$ at any particular position within the system.

σ_0. Master Sampler ignition slice. The boundary where spacetime becomes operational. Under the normalization $\sigma := \ln(\rho/\rho_0)$, the ignition slice has coordinate value $\sigma_0 \equiv 0$.

σ_1. First Nyquist–Shannon sampled scale-ring. Half-rate band edge; maximally aliased. Neutrino-sector hypothesis.

Scale-phase angle θ. The compact internal phase coordinate at each σ-slice, parameterising the $U(1)$ neighbor-scale bookkeeping. The KK compact coordinate is $y = R\theta$. Distinct from the noncompact render index σ.

Time dilation (STT). Scale-Flux slowdown caused by scale-upshift. Causal chain: scale-upshift → Scale-Flux slowdown → time dilation. The clock law is $d\tau/d\tau_0 = e^{-s_{\text{obs}}}$, where s_{obs} is the observer depth.

Truncated bipolar Fermat sweep. The pre-MSS carrier pattern: two opposite dipole branches curving outward in a Fermat-like spiral, cut off early by MSS ignition before extended visible winding accumulates. The important feature is the growing cumulative spectral burden ($C_H \propto \chi_H \rho^2$), not the number of visible turns or the local wavenumber.

Turbulent readout. Low-OSR regime where alias agitation dominates, perturbations amplify, and dynamics are quantum-heavy and stochastic.

PART 2 Mathematical Formalism

26 INTRODUCTION TO PART 2: THE DERIVATION LAYER

Part 1 defined STT as a reconstruction theory: a pre-geometric spectral carrier evolves on a punctured 2D scale plane; a rotating dipole source generates a truncated bipolar Fermat sweep whose growing cumulative spectral burden drives a representational crisis; and a discrete reconstruction mechanism (the Master Sampler) ignites at the critical scale ring as the minimum structure that restores readable output. Once the sampler exists, ticks define time, a lattice defines space, inverse Fourier synthesis defines readout, and filterless binning makes aliasing structurally unavoidable. From there, Scale-Flux slowdown generates OSR and the scale clock; render load produces scale-upshift and time dilation; electromagnetism appears as neighbor-scale phase bookkeeping; gravity appears as render-cost geometry sourced by the full bipolar reconstruction cycle; and the render stress tensor provides the accounting object needed for genuine field dynamics.

Part 2 formalizes that chain, without introducing interpretive layers that were not already committed in Part 1. Each equation appears only where it directly implements an already-named concept. Part 2 does not hide open problems inside ad hoc functional forms.

Completion-layer policy. Whenever a constitutive closure or empirical identification is required that goes beyond Part 1's conceptual commitments, Part 2 stops at the correct boundary and assigns the remainder to the completion layer. These boundaries are named explicitly so they cannot leak.

26.1 Epistemic Status (Strict)

To keep the manuscript internally honest, each mathematical move is tagged by its status:

Axiom (A): Primitive commitments of STT. **Derived result / theorem (D, T)**: Follows from axioms and definitions. **Calibration hypothesis (H)**: Identification of STT parameters with measured constants or datasets; not a derivation.

26.2 What Part 2 Locks Down

By the end of §44, the following are mathematically explicit:

A pre-MSS carrier on $\Sigma = \mathbb{R}^2\backslash\{0\}$ with a rotating bipolar drive and constant throughput sufficient to derive the unavoidable cumulative-burden ramp. MSS ignition as a representability boundary (cumulative spectral burden reaching C_{crit}), and aliasing as the resulting structural non-injectivity of filterless sampling. The discrete reconstruction architecture: ticks, cells, Nyquist bins, inverse Fourier readout, and a unitary Fourier-domain update yielding a well-de-

fined photon dispersion with maximal transport speed c_*. A Fourier-native bridge to the Schrödinger limit (as the post-MSS effective evolution of reconstructed fields), including the constraint that the carrier parameter fixes the emergent $\hbar$ once a slice is calibrated. The local KK phase-fiber model showing how a compact scale-phase coordinate supports a $U(1)$ connection and charge quantization in Kaluza–Klein form. The render stress tensor and a scale-coherence continuity law including σ-transport. The full bipolar reconstruction cycle with sector projectors, bipolar equipartition (A13), stationary burden symmetry (P6), and the conditional derivation of the sector-clock factor $s_{\text{geom}} = 2\, s_{\text{obs}}$ (C7). Gravity as scale-upshift sourced by the full-cycle burden, with the clock law and weak-field Schwarzschild matching (via the metric convention $g_{00} = e^{-s_{\text{geom}}}$) using the observer depth.

27 NOTATION AND MATHEMATICAL PRELIMINARIES

27.1 The Pre-MSS Arena

$\Sigma = \mathbb{R}^2 \setminus \{0\}$ with polar coordinates (ρ, ϕ), $\rho > 0$, $\phi \in [0,2\pi)$.

$\lambda \in \mathbb{R}$ is the strictly monotone ordering parameter.

27.2 Post-MSS Effective Coordinates

$X^A = (x^\mu, \sigma)$ with $A = 0,1,2,3,4$; $\mu = 0,1,2,3$; spatial indices $i, j = 1,2,3$.

$\sigma := \ln(\rho/\rho_0)$ is the dimensionless render index.

$y := R\theta$ is the compact scale-phase coordinate for the KK view, where $\theta \in [0,2\pi)$ is the internal phase at each σ-slice and R is the compactification radius. The render index σ remains noncompact.

27.3 Fourier Conventions

$k \in \mathbb{R}^3$ is the reconstructed spatial wavevector. $\mathscr{B} = [-\pi/\ell_0, \pi/\ell_0)^3$ is the Nyquist band / Brillouin zone.

27.4 Core Constants Reference

$c_* = \ell_0/\Delta t_*$, null-update transport speed.

Δt_*, Master Sampler tick period.

ℓ_0, fundamental lattice cell length.

ς, conserved pre-MSS constant (throughput/rotation ratio).

27.5 Convention on $\hbar$

The emergent identification $p = \hbar_{\text{eff}}\, k$ bridges lattice wavevectors to physical momentum. The value of $\hbar_{\text{eff}}$ is fixed by calibration in §35.

27.6 Ignition-Slice Convention

The ignition slice is denoted σ_0; under the normalization $\sigma := \ln(\rho/\rho_0)$, this slice has coordinate value $\sigma_0 \equiv 0$. Throughout Part 2, calculations use $\sigma = 0$ at ignition; the notation σ_0 is retained as the named label for this boundary in conceptual and cross-referencing contexts.

28 PRE-MSS CARRIER AND DIPOLE SOURCE

28.1 The Carrier Field

Axiom A1 (Carrier): A complex amplitude $F(\rho, \phi; \lambda) \in \mathbb{C}$ is defined on Σ, evolving in λ.

28.2 The Rotating Dipolar Boundary Drive

Axiom A2 (Bipolar drive). At the puncture $\rho \to 0$, the carrier is driven by a rotating bipolar boundary condition with factored form:

$$F(\rho, \phi; \lambda) \xrightarrow{\rho \to 0} A(\rho) \sum_{m \in \mathbb{Z}} h_m \, e^{im(\phi - \Omega\lambda)}, \qquad h_0 = 0, \quad \sum_{|m|=1} |h_m|^2 > 0$$

where Ω is the source rotation rate, the h_m are dimensionless, architecturally fixed shape coefficients, and $A(\rho)$ is the radial envelope. The constraints require: (i) mean-zero angular structure ($h_0 = 0$), and (ii) the first bipolar harmonic is present ($|h_1|^2 + |h_{-1}|^2 > 0$) and dominant, higher harmonics are permitted but sub-leading. The angular shape $H(\theta) = \sum_m h_m \, e^{im\theta}$ is part of the source's structural identity, not a tunable parameter.

Radial envelope convention. The radial envelope $A(\rho)$ is not an independent degree of freedom in the sense of altering the theory's predictions. It is constrained by the constant-throughput condition (Axiom A3) and by the normalization convention for ς; any residual freedom in $A(\rho)$ affects only the overall amplitude of the carrier, which is absorbed into the definition of ς and the representability threshold $C_{\text{crit}}2$. The envelope therefore carries no additional free data that changes the ignition scale or the burden law beyond what ς, χ_H, and C_{crit} already determine.

Minimal first-harmonic source. In the minimal realization, only $h_{\pm 1} \neq 0$:

$$H(\theta) = h_1 \, e^{i\theta} + h_{-1} \, e^{-i\theta}$$

The simplest real bipolar mode is $H(\theta) = \cos\theta$ (i.e., $h_1 = h_{-1} = \frac{1}{2}$). This is the leading-order content of any smooth bipolar source.

Source-shape factor. The effective spectral writing rate depends not only on the rotation rate Ω but also on the harmonic content of the fixed angular shape. Define the source-shape factor:

$$\chi_H := \frac{\sum_{m\neq 0} m^2 \, |h_m|^2}{\sum_{|m|=1} |h_m|^2}$$

The denominator is the first-harmonic power $|h_1|^2 + |h_{-1}|^2$. By construction:

- For any pure first-harmonic source (including $H = \cos\theta$): $\chi_H = 1$.
- For a source with higher harmonics: $\chi_H > 1$.
- χ_H depends only on the fixed shape coefficients h_m, not on the radial envelope $A(\rho)$ or on position.

The quadratic growth of cumulative burden (§30) and the existence of MSS ignition (§31) are universal, they hold for any bipolar source. The source-shape factor sets only the prefactor of the cumulative burden, and therefore shifts the ignition radius quantitatively but not the existence of ignition itself.

Finite-core regularization. The puncture-dipole boundary condition is the far-field / zero-core limit of a more intuitive finite-core source: a regularized rotating two-lobed source profile on a small finite core, producing a yin-yang-like rotating bipolar morphology. The current equations use the zero-core limit; the finite-core regularization yields the same far-field carrier and the same cumulative-burden scaling ($C_H \propto \chi_H \, \rho^2$). All downstream formal derivations are carried out in the zero-core limit; finite-core regularization changes the ignition radius by a small offset but does not alter the ρ^2 scaling or the downstream zero-core structure.

Source-ansatz interpretation. The boundary drive of A2 is most naturally read as the harmonic decomposition of a rotating bipolar angular pattern rather than as two independent emitters. A general source ansatz is a rotating two-lobed angular profile

$$S(\phi, \lambda) = S_0 \, H(\phi - \Omega\lambda),$$

where H is 2π-periodic, bipolar, and mean-zero. The simplest realization is $H(\theta) = \cos\theta$ ($\chi_H = 1$). The yin-yang picture corresponds to a smoother nonlinear choice of H that includes higher harmonics ($\chi_H > 1$) while preserving the same bipolar topology. The choice of H is architecturally fixed; it affects the prefactor of the cumulative burden (via χ_H) but not the ρ^2 scaling law or the existence of ignition.

This makes explicit that the source is a single coherent rotating bipolar excitation with two phase-opposed lobes, a balanced rotating phase topology, not two discrete pre-geometric objects.

Because the source keeps rotating while its inscription is carried outward, the two branches immediately curve into a Fermat-like spiral pattern. The MSS ignites early (at ρ_0, where the cumulative spectral burden reaches the representability threshold), so the pre-MSS carrier is a truncated bipolar Fermat sweep rather than a fully developed multi-turn spiral.

29 SCALE FLUX AS CONSTANT THROUGHPUT: MINIMAL EXPLICIT LAW

29.1 Constant Area Flux

Axiom A3 (Constant area throughput): The outward flux through any closed curve encircling the origin on Σ is constant:

$$\oint \mathbf{J} \cdot \hat{n}\, d\ell = \text{const} = \varsigma \cdot \Omega$$

29.2 Radial Slowdown

Derived result D1 (Radial slowdown): From A3, in radial symmetry:

$$J_\rho(\rho) = \frac{\varsigma\, \Omega}{2\pi\rho}$$

The flux velocity decreases as $1/\rho$, or equivalently $\propto e^{-\sigma}$ in render-index coordinates. Scale Flux decelerates with increasing scale depth.

29.3 The Conserved Pre-MSS Constant ς

$\varsigma =$ (throughput rate)/(rotation rate). The source profile H (and its shape factor χ_H) is fixed architecturally as part of the source's structural identity. Given that fixed profile, ς is the single free parameter of the pre-MSS regime. Together with χ_H, it fixes the geometry of the carrier's spectral content and determines where the distribution limit will be reached.

30 THE UNAVOIDABLE PHASE-CROWDING RAMP

30.1 Cumulative Spectral Burden

The flux velocity $J_\rho(\rho) \propto 1/\rho$ (D1) decreases outward, so the local phase gradient at any single radius also decreases with radius. The phase-crowding ramp is therefore not a local-gradient effect. The correct monotone crowding variable is the cumulative spectral burden: the total spectral inventory inscribed in the carrier up to radius ρ.

The transit time across a radial increment $d\rho$ at radius ρ is:

$$d\lambda = \frac{d\rho}{J_\rho(\rho)} = \frac{2\pi\rho}{\varsigma\,\Omega}\,d\rho$$

During this ordering-parameter interval, the source rotates by $d\phi_{\text{source}} = \Omega\,d\lambda$. For a general bipolar source with shape factor χ_H (§28.2), the effective spectral writing rate is amplified by the harmonic content of the source profile. The cumulative spectral burden inscribed between a small inner cutoff ϵ (the finite-core regularization radius; §28.2) and radius ρ is:

$$C_H(\rho) = \frac{\pi\,\chi_H}{\varsigma}\left(\rho^2 - \epsilon^2\right)$$

In the zero-core limit $\epsilon \to 0$, this becomes $C_H(\rho) = \pi\chi_H\rho^2/\varsigma$. For the minimal first-harmonic source ($\chi_H = 1$), this reduces to $C(\rho) = \pi\rho^2/\varsigma$.

30.2 Ramp as Cumulative Burden Growth

Theorem T1 (Unavoidable ramp). Under A1–A3, the cumulative spectral burden of the carrier grows without bound:

$$C_H(\rho) \;\propto\; \chi_H\,\rho^2 \;\to\; \infty \quad \text{as}\,\rho \to \infty$$

In render-index coordinates ($\sigma = \ln(\rho/\rho_0)$):

$$C_H(\sigma) \;\propto\; \chi_H\,e^{2\sigma}$$

Derivation. From A3, $J_\rho = \varsigma\Omega/(2\pi\rho)$. The ordering-parameter cost per unit radius is $d\lambda/d\rho = 1/J_\rho = 2\pi\rho/(\varsigma\Omega)$. The source (A2) inscribes spectral content at a rate proportional to $\Omega\chi_H$ during that interval. Integration gives $C_H(\rho) \propto \chi_H\,\rho^2$. Since the integrand is positive

and $\chi_H > 0$, C_H is strictly monotone increasing for any bipolar source profile. The ρ^2 scaling is universal; the source-shape factor χ_H sets only the prefactor. □

The ramp is not optional; it is a necessary consequence of constant throughput and coherent bipolar drive. The carrier accumulates more and more inscribed spectral content with increasing radius, even though the local wavenumber at any single radius is decreasing. What saturates the readout is this cumulative burden, not the local spectral density. The truncated bipolar Fermat sweep is the geometric realisation of this growing burden.

31 DISTRIBUTION LIMIT AND MSS IGNITION

31.1 Representability Threshold

Axiom A4 (Finite representability): There exists a critical cumulative burden C_{crit} beyond which continuous pointwise readout of the carrier becomes ill-posed.

31.2 Ignition Condition

Axiom A5 (Ignition trigger): MSS ignition occurs at the critical radius ρ_0 where $C_H(\rho_0) = C_{\text{crit}}$.

Zero-core convention. From this point onward, the formal derivation adopts the zero-core limit $\epsilon \to 0$ (§28.2), so $C_H(\rho) = \pi\chi_H\rho^2/\varsigma$. The finite-core regularization shifts the ignition radius to $\rho_0 = \sqrt{\epsilon^2 + \varsigma C_{\text{crit}}/(\pi\chi_H)}$, but the correction is negligible for $\epsilon \ll \rho_0$ and does not affect downstream results within the adopted zero-core formalism.

Derived result D2 (Ignition scale, zero-core limit). Combining T1 with A5 in the zero-core limit:

$$\rho_0 = \sqrt{\frac{\varsigma\, C_{\text{crit}}}{\pi\, \chi_H}}$$

The ignition scale is fully determined by the pre-MSS constant ς, the representability threshold C_{crit}, and the architecturally fixed source-shape factor χ_H. A richer bipolar profile ($\chi_H > 1$) accumulates burden faster and therefore ignites at a smaller radius than the minimal first-harmonic source.

31.3 Operational Meaning of the Distribution Limit

At ρ_0, the cumulative spectral burden of the source-written carrier exceeds what any continuous readout can resolve. The carrier has accumulated too much spectral inventory, not because the local wavenumber is high (it is actually decreasing with radius), but because the shape-weighted cumulative burden written by the rotating source grows as $\chi_H\,\rho^2$. Beyond ρ_0, the carrier's radial structure becomes distributional, ill-posed as a pointwise function. The Master Sampler ignites at this ring as the earliest discrete architecture capable of stabilizing what the dipole source has already made unavoidable.

31.4 The Regularized Pre-Limit Trace

The distribution limit is a statement about the carrier's radial structure at ρ_0: the radial profile $F(\rho, \phi; \lambda)$ ceases to be pointwise representable as a function of ρ at and beyond ρ_0. The angular trace at ρ_0, the restriction of F to the circle at fixed radius, need not be distributional in the angular variable ϕ.

Nevertheless, to avoid any ambiguity at the boundary itself, the MSS input is defined as the regularized pre-limit trace: the carrier evaluated infinitesimally inside the ignition ring:

$$g(\phi; \lambda) := \lim_{\rho \to \rho_0^-} F(\rho, \phi; \lambda)$$

Regularity assumption. We assume that $F(\rho, \phi; \lambda)$, viewed as a function of ϕat fixed λ, has a well-defined left limit as $\rho \to \rho_0^-$ for each angular position ϕ. This is a regularity condition on the carrier: the distribution limit at ρ_0 concerns the radial structure (the radial profile ceases to be pointwise representable), but the angular trace remains regular up to the boundary. This assumption is natural for the smooth bipolar sources of A2 but is not derived from A1–A5; it is an additional regularity postulate. The sampler reads the last well-posed angular trace before the radial crisis, not the distributional object at the boundary itself.

This is the operational content of the "ring-trace arrival signal": the angular structure of the carrier at the approach to the ignition ring, delivered to the MSS as its sole causal input from the pre-geometric regime.

31.5 Bridge to Post-MSS Readout

The ignition ring ρ_0 serves a dual role: it is both the radius where continuous radial readout fails and the boundary at which the MSS reads its angular input. The crisis variable (cumulative spectral burden $C_H(\rho)$) and the sampled variable (angular coefficients $c_{m,n}$) are connected by this shared boundary: the angular complexity at ρ_0^- is the spectral content that the cumulative burden has delivered to the approach of that ring. The MSS discretises this angular content; it does not attempt to extend the radial readout beyond the distribution limit.

32 MSS ARCHITECTURE: TICKS, CELLS, BINS, AND FOURIER READOUT

32.1 Ticks and Lattice

Axiom A6 (Discrete ticks): Post-MSS, evolution is indexed by $n \in \mathbb{Z}$, with tick-sampled ordering-parameter values λ_n.

The reconstructed spatial lattice is $\Lambda = \ell_0 \mathbb{Z}^3$. At each tick n, the sampler produces a sector-valued field on this lattice:

$$\Psi_n : \Lambda \to \mathscr{R} \otimes \mathbb{C} \;\cong\; \mathbb{C}^8$$

where $\mathscr{R}$ is the 8-dimensional real closure space (§37.1), $\dim(\mathscr{R}) = 8$, and the complexification arises because the Fourier readout machinery (A7, A8) operates on complex amplitudes. The underlying real structure $\mathscr{R}$ carries the closure algebra and sector projectors P_{q_+}, P_{q_-} (§37.2); the complex representation $\mathbb{C}^8$ is chosen for convenience in spectral synthesis. The dimensionality relevant for capacity counting is the real dimension $\dim(\mathscr{R}) = 8$.

Scalar reduction convention. The Fourier readout, aliasing, dispersion, and OSR machinery of §§32–36 operate identically on each component of Ψ_n. For notational clarity, these sections are written in terms of a single-component scalar field $\psi_n(x) \in \mathbb{C}$, understood as the projection of Ψ_n onto any one closure direction. All equations generalise to the full sector-valued case by applying them component-wise. The lift map $\mathscr{L}$, alias sum (A7), Fourier readout (A8), and unitary update (A9) act on each component independently; cross-component coupling enters only through the bipolar cycle operators U_{q_+}, U_{q_-} of §37.2. The observable 4D readout is ultimately the q_+-projected component $P_{q_+}\Psi_n$; the scalar ψ_n used in §§32–36 can therefore be understood as a representative component of this projected sector.

Post-MSS coordinates: $\sigma := \ln(\rho/\rho_0)$, so $\sigma = 0$ at the ignition ring (σ_0) and σ_1 denotes the first Nyquist–Shannon sampled scale-ring.

Definition (Ring-trace arrival signal). The sampler's incoming signal is the regularized pre-limit trace of the carrier at the approach to the MSS ignition ring (§31.4):

$$g(\phi;\lambda) := \lim_{\rho \to \rho_0^-} F(\rho,\phi;\lambda), \quad \phi \in [0,2\pi)$$

This is a well-defined function of ϕ by the regularity assumption of §31.4: the distribution limit concerns the radial structure at ρ_0, while the angular trace remains regular up to the boundary.

Definition (Tick-sampled ring-trace). Post-MSS, ticks define sampling times along the ordering parameter:

$$g_n(\phi) := g(\phi; \lambda_n)$$

Definition (Angular projection). At each tick the sampler performs an angular Fourier projection of the tick-sampled arrival trace:

$$c_{m,n} := \frac{1}{2\pi} \int_0^{2\pi} g_n(\phi)\, e^{-im\phi}\, d\phi, \quad m \in \mathbb{Z}$$

This integral is well-defined because $g_n(\phi)$ is an ordinary function on S^1 (the pre-limit trace), not the distributional object at the boundary itself.

32.2 Nyquist Binning Without Anti-Alias Filtering

Definition (Lift map and pre-alias lifted spectrum). The tick-indexed angular-projection coefficients $\{c_{m,n}\}$ seed a pre-alias lifted spectrum on $\mathbb{R}^3$ via a fixed architectural lift map $\mathscr{L}$:

$$\hat{\Psi}_{\mathrm{lift},n}(k) := (\mathscr{L}\{c_{m,n}\})(k), \quad k \in \mathbb{R}^3$$

Axiom A7 (Filterless binning): The sampler applies no anti-alias prefilter. The stored spectral coefficient at each $k \in \mathscr{B}$ is the alias sum of the lifted spectrum over the full lattice reciprocal cell:

$$\hat{\psi}_{\mathrm{store},n}(k) = \sum_{q \in \mathbb{Z}^3} \hat{\Psi}_{\mathrm{lift},n}\left(k + \frac{2\pi}{\ell_0} q \right), \quad k \in \mathscr{B}$$

High-frequency content is not removed; it folds additively into the representable band. This is the operational form of Part 1 §5.4's crucial onset condition: the Master Sampler ignites without an anti-alias filter. Aliasing is therefore structurally unavoidable from the first tick onward.

Pipeline summary. The complete per-tick spectral path is:

$$g_n(\phi) \xrightarrow{\text{angular projection}} \{c_{m,n}\} \xrightarrow{\mathscr{L}} \hat{\Psi}_{\mathrm{lift},n}(k) \xrightarrow{\text{alias sum (A7)}} \hat{\psi}_{\mathrm{store},n}(k)$$

32.3 Inverse Fourier Synthesis

Axiom A8 (Fourier readout): Each tick's readout is synthesized from the stored (alias-summed) bins:

$$\psi_n(x) = \int_{\mathscr{B}} \hat{\psi}_{\mathrm{store},n}(k)\, e^{ik\cdot x}\, \frac{d^3k}{(2\pi)^3}, \quad x \in \Lambda$$

On each tick, the sampler "draws" physical space by summing its stored harmonics into a reconstructed pattern. Because $\hat{\psi}_{\mathrm{store},n}$ already contains folded high-frequency contributions (A7), the readout inherently encodes alias content.

33 ALIASING AS STRUCTURAL NON-INJECTIVITY

33.1 Aliasing Equivalence Classes

Two underlying spectra $\hat{\Psi}$, $\hat{\Phi}$ produce the same stored bins (and therefore the same readout) whenever their alias sums agree:

$$\hat{\Psi} \sim \hat{\Phi} \iff \sum_{q\in\mathbb{Z}^3} \hat{\Psi}\left(k + \frac{2\pi}{\ell_0} q\right) = \sum_{q\in\mathbb{Z}^3} \hat{\Phi}\left(k + \frac{2\pi}{\ell_0} q\right) \quad \text{for all } k \in \mathscr{B}$$

Derived result D3 (Non-injectivity). The map "underlying spectral content → alias-summed stored bins → reconstructed field" is not injective in a filterless sampler. Multiple distinct underlying configurations produce the same readout. A quantum state does not have a unique classical trajectory because the sampler's finite resolution makes multiple underlying realities compatible with the same reconstructed output.

This is the formal statement of Part 1's identification of aliasing with quantum indeterminacy: the irreducible ambiguity of quantum mechanics is not a feature of reality itself but of a filterless reconstruction that cannot distinguish spectrally folded configurations.

33.2 The Fourier Uncertainty Bound (Base Theorem)

For bandlimited states, the standard Fourier uncertainty inequality holds:

$$\Delta x \, \Delta k \gtrsim \frac{1}{2}$$

With the emergent identification $p = \hbar_{\text{eff}} \, k$:

$$\Delta x \, \Delta p \gtrsim \frac{\hbar_{\text{eff}}}{2}$$

34 UNITARY TICK UPDATE AND PHOTON DISPERSION

34.1 Unitary Fourier-Domain Evolution

Axiom A9 (Unitary update): The stored spectral bins evolve by a unitary multiplier:

$$\hat{\psi}_{n+1}(k) = U(k)\,\hat{\psi}_n(k), \quad |U(k)| = 1, \quad k \in \mathscr{B}$$

Write $U(k) = e^{-i\omega(k)\Delta t_*}$, defining a dispersion $\omega(k)$ and baseline tick interval Δt_*.

$c_* := \ell_0/\Delta t_*$ is the null-update transport speed, the sampler's intrinsic conversion ratio between spatial steps and time ticks.

Continuum-limit convention: The fundamental dynamics are discrete: ticks $n \in \mathbb{Z}$, lattice cells spaced by ℓ_0, unitary update $\hat{\psi}_{n+1} = U\hat{\psi}_n$. Throughout Part 2, whenever continuous derivatives appear (∂_t, ∇^2, PDEs), they denote the long-wavelength, long-time continuum limit.

34.2 Massless Lattice Dispersion and Maximal Speed c_x

A lattice-causal choice of dispersion is:

$$\omega_\gamma(k) = \frac{2c_*}{\ell_0}\left[\sum_{j=1}^{3}\sin^2\left(\frac{k_j\ell_0}{2}\right)\right]^{1/2}$$

Derived result D4 (Continuum limit): For $|k|\ell_0 \ll 1$:

$$\omega_\gamma(k) \;\to\; c_*\,|k|$$

This is the standard massless dispersion relation, recovering photon-like propagation in the long-wavelength limit.

Derived result D5 (Bounded group velocity): The group velocity satisfies $|v_g| \le c_*$. Thus c_* is the maximal null-transport speed of phase information across the reconstructed lattice.

34.3 Spherical Wavefronts and the Photon's σ-Envelope

The continuum-limit dispersion implies the standard massless wave equation. For a localized emission event, the outgoing solution takes the spherical Green's function form, and constant

phase is $r = c_* t$, a photon emitted from a localized event is geometrically an outgoing null phase wavefront, an expanding spherical shell in the 3D spatial slice.

35 CARRIER EVOLUTION AND THE SCHRÖDINGER LIMIT

35.1 Quadratic Spectral Phase Evolution (Massive Sector)

Axiom A10 (Quadratic evolution for massive reconstructed modes): For modes with $|k|\ell_0 \ll 1$, the dispersion acquires a quadratic (massive) correction:

$$\omega(k) = \omega_0 + \frac{c_* k^2}{2\mu}$$

where μ is a mass-scale parameter.

35.2 Bridge to Far-Field Reference Time

The quadratic dispersion of A10 contains a mass-scale parameter μ. To connect the lattice formalism to physical observables, two calibration hypotheses fix the mapping from lattice parameters to measured constants:

Calibration hypothesis H1 (Mass scale in a chosen slice). In a chosen σ-slice, the mass parameter μ is identified with the electron mass: $\mu = m_e c_*/\hbar_{\text{eff}}$, fixing the emergent mass scale.

Calibration hypothesis H2 (Planck-constant verification). The emergent $\hbar_{\text{eff}}$ defined by the lattice Fourier uncertainty relation ($\Delta x\, \Delta p \geq \hbar_{\text{eff}}/2$, §33.2) is identified with the measured $\hbar$. This is not independently adjustable once ℓ_0, Δt_*, and c_* are fixed; it serves as a consistency check that the lattice parameters reproduce quantum mechanics in the continuum limit.

Together, H1 and H2 anchor the lattice formalism to observed particle physics: m_e sets the mass scale, and $\hbar$ confirms the momentum-position uncertainty structure.

35.3 Clock Structure: Baseline Tick Time, Far-Field Time, and Local Proper Time

The baseline tick time is Δt_*, the MSS's fundamental period. The far-field reference time is the tick time at a given render index σ, where no scale-upshift is present:

$$d\tau_0(\sigma) = \frac{\Delta t_*}{\text{OSR}(\sigma)}$$

Proper time from the metric convention. The geometric depth $s_{\text{geom}}(x)$ enters the emergent 4D metric through the temporal component (§40):

$$g_{00} = e^{-s_{\text{geom}}}$$

For a stationary observer in this metric, the proper-time ratio follows from the standard relation:

$$\frac{d\tau}{d\tau_0} = \sqrt{g_{00}} = e^{-s_{\text{geom}}/2}$$

Using the sector-clock relation $s_{\text{obs}} = s_{\text{geom}}/2$ (Conditional Result C7, §37.5):

$$\frac{d\tau}{d\tau_0} = e^{-s_{\text{obs}}}$$

In the weak-field regime (§40.3–40.4), this yields $d\tau/d\tau_0 \approx 1 + \Phi_N/c_*^2$, matching the standard GR coefficient.

Why the clock law does not follow from raw OSR ratios. One might expect the proper-time ratio to equal the OSR ratio $\text{OSR}(\sigma)/\text{OSR}(\sigma + s_{\text{geom}}) = e^{-2s_{\text{geom}}}$. That ratio measures the **full-cycle reconstruction overhead**, how much more sampling work the shifted location requires. It is not the observable clock rate. The observable clock rate is the q_+-projected readout, which is governed by the emergent metric, not by the raw reconstruction ratio. The connection between OSR and proper time is qualitative (higher $s_{\text{geom}} \to$ higher OSR $\to$ more classical) but the quantitative clock law is set by the metric convention and the sector-clock theorem, not by taking OSR ratios directly. In short: OSR tracks reconstruction stability, while the metric (and thus the clock law) tracks the effective geometry that this stability produces; the two are correlated but not quantitatively identical.

Ontological clarification. When Part 1 says "proper time is the local scale-clock rate," the precise meaning is: the observable scale clock is the q_+-projected, metric-dressed cadence $d\tau/d\tau_0 = e^{-s_{\text{obs}}}$, not the bare reconstruction-overhead ratio $e^{-2s_{\text{geom}}}$. The bare OSR ratio governs how much sampling work is required; the observable clock is the metric response of that work as seen by the projected sector. This distinction is what prevents the factor-of-two from being "read off" from raw OSR ratios and is why the sector-clock theorem (C7) is needed.

36 RENDER INDEX, SCALE CLOCK, AND OSR

36.1 Mapping Scale Depth to Render Index

The render index $\sigma := \ln(\rho/\rho_0)$ maps the continuous radial coordinate to a dimensionless logarithmic depth.

36.2 Minimal Explicit Slowdown Law

The minimal area-throughput realization of the Scale-Flux Velocity Law gives:

$$\frac{d\sigma}{d\lambda} \propto e^{-2\sigma}$$

36.3 OSR Definition

Define:

$$d\tau_0(\sigma) = \frac{\Delta t_*}{\mathrm{OSR}(\sigma)}$$

where $\nu(\sigma) := \nu_0 \, d\sigma/d\lambda$ with ν_0 a proportionality constant. Then:

$$\mathrm{OSR}(\sigma) = \frac{\nu_{\mathrm{MSS}}}{\nu_0} \left(\frac{d\sigma}{d\lambda} \right)^{-1}$$

Under the minimal slowdown law, $d\sigma/d\lambda \propto e^{-2\sigma}$, so:

$$\mathrm{OSR}(\sigma) \propto e^{2\sigma}$$

OSR grows exponentially with render index: deeper scales dwell longer, accumulate more sampling updates per meaningful change, and produce progressively more classical readout.

36.4 Scale-Upshift Field: Geometric and Observer Depths

Represent scale-upshift by a field $s_{\mathrm{geom}}(x)$ that shifts the effective render index. The full-cycle geometric depth is:

$$\sigma_{\mathrm{eff}}(x) = \sigma + s_{\mathrm{geom}}(x)$$

so:

$$\mathrm{OSR}(x) = \mathrm{OSR}(\sigma_{\mathrm{eff}}(x))$$

The geometric depth sources geometry and responds to the full bipolar burden $B = q_+ + q_-$.

The observer depth is the projected-sector depth governing measured clocks:

$$s_{\mathrm{obs}}(x) = \frac{1}{2}\, s_{\mathrm{geom}}(x)$$

The clock law is:

$$\frac{d\tau}{d\tau_0} = e^{-s_{\mathrm{obs}}}$$

This is the formal realization of Part 1's sector-clock architecture. The relation $s_{\mathrm{obs}} = s_{\mathrm{geom}}/2$ is derived as Conditional Result C7 (§37.5) from bipolar equipartition, stationary burden symmetry, the observer source law, and shared linearised coupling: geometry feels the full two-part cycle; the observer measures only one effective half-cycle.

37 CLOSURE AND THE BIPOLAR RECONSTRUCTION CYCLE

37.1 Internal Closure Cap and State Space

Axiom A11 (Closure cap): Each cell carries an internal bookkeeping state with eight independent directions.

The internal closure space is an 8-dimensional real vector space $\mathscr{R}$, $\dim(\mathscr{R}) = 8$, consistent with octonionic algebra. The projectors P_{q_+}, P_{q_-} are orthogonal projectors on this real space. The operational field $\Psi_n(x) \in \mathscr{R} \otimes \mathbb{C} \cong \mathbb{C}^8$ (§32.1) lives in the complexified closure space; the complex basis is chosen for convenience in spectral synthesis (Fourier readout operates on complex amplitudes). The dimensionality relevant for capacity counting is the real dimension $\dim(\mathscr{R}) = 8$.

Burden capacity. For a projector P onto a subspace of $\mathscr{R}$, its capacity $C_P = \dim(P\mathscr{R})$ is the number of independent closure dimensions allocated to that subspace. This is the total available capacity; the render burden density ρ_R of §39.1 measures how much of that capacity is actively being used at a given point and scale.

37.2 Bipolar Reconstruction Cycle

Axiom A12 (Bipolar operator splitting): The full reconstruction cycle per tick is:

$$\Psi_{n+1} = U_{q_-} U_{q_+} \Psi_n$$

with orthogonal projectors P_{q_+} and P_{q_-} satisfying:

$$P_{q_+}^2 = P_{q_+}, \quad P_{q_-}^2 = P_{q_-}, \quad P_{q_+} P_{q_-} = P_{q_-} P_{q_+} = 0, \quad P_{q_+} + P_{q_-} = I$$

$$P_{q_+}^\dagger = P_{q_+}, \quad P_{q_-}^\dagger = P_{q_-}$$

Electromagnetic $U(1)$ link phases act dominantly on q_+-sector degrees of freedom:

$$\Psi \;\mapsto\; e^{iq\theta(x)} P_{q_+} \Psi + P_{q_-} \Psi$$

Explicit cross-sector coupling suppression (the mechanism by which the q_- sector becomes EM-invisible in q_+ readout) is deferred to the completion layer.

37.3 Bipolar Equipartition

Axiom A13 (Bipolar equipartition). Stable operation of the Master Sampler requires that the two sectors have equal closure capacity:

$$\dim(P_{q_+}\mathscr{R}) = \dim(P_{q_-}\mathscr{R}) = \tfrac{1}{2}\dim(\mathscr{R}) = 4$$

In the absence of an exchange symmetry that forces equal dimensions, an unequal split would generically lead to a net drift per cycle, accumulating over many ticks. The octonionic closure is minimal and symmetric; the only stable, non-fine-tuned split is the equal one. Deriving this from deeper principles (e.g., a variational principle or explicit exchange symmetry) is completion-layer work.

37.4 Stationary Burden Symmetry

Define the local sector burden densities from the reconstruction state:

$$b_{q_+}(x) := \langle \Psi(x) \,|\, P_{q_+} \,|\, \Psi(x) \rangle_{\text{render}}, \qquad b_{q_-}(x) := \langle \Psi(x) \,|\, P_{q_-} \,|\, \Psi(x) \rangle_{\text{render}}$$

These are pointwise densities at each spacetime location, not integrated totals.

Postulate P6 (Stationary burden symmetry, local form). For any stationary configuration that does not spontaneously break the symmetry of the bipolar cycle, the local render burden densities in the two sectors are equal at each point:

$$b_{q_+}(x) = b_{q_-}(x) \quad \text{for all } x$$

The cycle operator acts independently on the two sectors. If the state had unequal local weights, the cycle would generally rotate it within the larger-weight sector unless the unitary operators were specifically chosen to cancel the effect at every point. For a stationary state that is generic (not fine-tuned), the natural configuration is one that respects the exchange symmetry between the two sectors pointwise, leading to equal local densities. A full derivation would require an explicit exchange symmetry operator, which is not yet present in the axioms; therefore this is taken as a postulate, to be derived later.

The total local burden density sourcing the geometric field is:

$$b_{\text{tot}}(x) = b_{q_+}(x) + b_{q_-}(x) = 2\, b_{q_+}(x)$$

The integrated sector burdens $B_{q_\pm} := \int b_{q_\pm}(x)\, d^3x$ inherit the equality from the local form.

37.5 The Sector-Clock Theorem (Conditional Derivation)

The factor-of-two is derived under four explicit conditions: (i) symmetric closure capacity (A13), which provides the architectural precondition making sector symmetry natural; (ii) equal local sector burden densities in the stationary state (P6, local form); (iii) the observer source law (C7-ii), which posits that the q_+-projected clock responds to q_+-sector burden through the same linear operator as geometry responds to total burden; and (iv) shared linearised coupling and boundary conditions (C7-iii). The algebraic derivation uses P6, C7-ii, and C7-iii directly; A13 enters as the structural reason why P6 is a natural rather than fine-tuned assumption. All four are stated below.

The derivation of $s_{\text{geom}} = 2\, s_{\text{obs}}$ requires the following assumptions, all stated explicitly:

Assumption C7-i (Geometric source law). The geometric depth $s_{\text{geom}}(x)$ satisfies the linearised Poisson equation sourced by the total render burden density (§40.0–40.1):

$$\nabla^2 s_{\text{geom}} = -\,\kappa_s\, b_{\text{tot}}$$

Assumption C7-ii (Observer source law). The observer depth $s_{\text{obs}}(x)$, which governs the clock rate in the q_+-projected sector, satisfies the same linearised Poisson equation sourced by the visible-sector burden density only:

$$\nabla^2 s_{\text{obs}} = -\,\kappa_s\, b_{q_+}$$

This is a separate postulate: it asserts that the q_+-projected clock responds to the q_+-sector burden through the same render-cost operator that governs the geometric field. It is natural in the linearised regime (both fields are responses to the same underlying render-cost mechanism at leading order), but it is not derived from A13 or P6. Deviations at higher order are deferred to the completion layer.

Assumption C7-iii (Shared coupling and boundary conditions). The same coupling constant κ_s and the same boundary conditions (vanishing at infinity) apply to both s_{geom} and s_{obs}.

Derivation. Given A13 (bipolar equipartition) and P6 (stationary burden symmetry, local form), $b_{\text{tot}}(x) = 2\, b_{q_+}(x)$ pointwise. Then:

$$\nabla^2 s_{\text{geom}} = -\,\kappa_s\,(2\, b_{q_+}) = 2\,\nabla^2 s_{\text{obs}}$$

With shared boundary conditions, the solutions are proportional:

Conditional Result C7 (Sector-clock factor). Given bipolar equipartition (A13), stationary burden symmetry (P6), the observer source law (C7-ii), and shared linearised coupling (C7-iii):

$$s_{\mathrm{geom}} = 2\, s_{\mathrm{obs}}$$

The factor-of-two is not an arbitrary numerical patch. It is a conditional consequence of the symmetric bipolar architecture together with the assumption that both depth fields respond to their respective sector burdens through the same linearised render-cost operator. Observable proper time is measured in the q_+-projected readout sector:

$$\frac{d\tau}{d\tau_0} = e^{-s_{\mathrm{obs}}}, \quad s_{\mathrm{obs}} = \tfrac{1}{2}\, s_{\mathrm{geom}}$$

where s_{geom} is the solution to the geometric field equation (§40) sourced by the full bipolar burden.

38 THE KALUZA–KLEIN PHASE-FIBER MODEL: U(1) FROM SCALE PHASE

38.1 Compact Scale-Phase Coordinate

The render index σ is noncompact and monotone, it orders the scale-ring ladder, supports epoch structure, and carries $\mathrm{OSR}(\sigma) \propto e^{2\sigma}$. It cannot be compactified without destroying these global features.

The KK construction operates on a separate compact coordinate: the scale-phase angle $\theta \in [0,2\pi)$, which parameterises the local angular bookkeeping at each σ-slice. This is the periodic internal phase that the sampler maintains for neighbor-scale consistency. Define:

$$y := R\,\theta, \quad y \sim y + 2\pi R$$

where R is the compactification radius. The coordinate y is the compact internal phase; σ remains noncompact.

Dimensional structure. The global STT effective arena is $3 + 1 + \sigma$: four reconstructed spacetime dimensions plus the noncompact render index. Electromagnetism is represented by the compact internal phase fiber θ at each σ-slice. The KK construction is a fiber-bundle-style local reformulation, it treats the phase fiber as a local fifth coordinate (x^μ, y) at fixed σ, not an additional global spacetime dimension. The full coordinate structure is therefore $3 + 1 + \sigma$ (global arena) with a compact θ-fiber (local KK phase) attached at each slice.

Important distinction: The KK reformulation is a local effective model that captures the $U(1)$ phase structure at a given σ-slice. It does not compactify the global render index. The KK circle y encodes neighbor-scale phase transport; the noncompact σ encodes the scale-ring ladder, epoch ordering, and OSR scaling. These are different objects.

38.2 KK Metric Ansatz

Use the standard Kaluza–Klein form:

$$ds^2 = g_{\mu\nu}(x)\,dx^\mu dx^\nu + \Phi_{\mathrm{KK}}^2(x)\big(dy + \kappa_{\mathrm{KK}}\,A_\mu(x)\,dx^\mu\big)^2$$

In STT terms: $\Phi_{\mathrm{KK}}(x)$ is the KK radion/dilaton scalar, related to the geometric scale-upshift field by $\Phi_{\mathrm{KK}}(x) = e^{s_{\mathrm{geom}}(x)}$; in weak field ($|s_{\mathrm{geom}}| \ll 1$), $\Phi_{\mathrm{KK}} \approx 1 + s_{\mathrm{geom}}$. $A_\mu(x)$ is the neighbor-scale phase connection (electromagnetism). $g_{\mu\nu}(x)$ is the emergent 4D metric in the high-OSR regime. κ_{KK} is the KK coupling constant.

Zero-mode truncation: $g_{\mu\nu}$, Φ_{KK}, and A_μ are taken y-independent. Higher KK harmonics correspond to massive modes and are deferred to the completion layer.

38.3 Mode Number and Charge Quantization

Expand a field in harmonics around the compact phase circle:

$$\Psi(x,y) = \sum_{n\in\mathbb{Z}} \psi_n(x)\, e^{iny/R}$$

The fifth momentum is quantized: $p_5 = n\hbar_{\mathrm{eff}}/R$.

KK reduction produces an effective coupling: $q_n \propto \kappa_{\mathrm{KK}}\, p_5 = \kappa_{\mathrm{KK}}\, n\hbar_{\mathrm{eff}}/R$.

Derived result D6 (Quantized charge labels): The coupling is integer-labeled by n. Positive and negative n correspond to opposite winding orientations, positive and negative charge.

Calibration hypothesis H3: Fix the unit by matching the elementary charge e.

39 RENDER STRESS TENSOR AND SCALE-COHERENCE CONSERVATION

39.1 Render Stress Tensor on $3 + 1 + \sigma$

Define a symmetric tensor $T_R^{AB}(x^\mu, \sigma)$ on the global $3 + 1 + \sigma$ arena (not the KK phase fiber) that encodes burden density, spatial flows and stresses, and scale transport:

$$\rho_R := T_R^{00}, \quad J^i := T_R^{0i}, \quad J^\sigma := T_R^{04}$$

ρ_R: render burden density. J^i: spatial burden current. J^σ: scale transport current along σ.

39.2 Scale Coherence as Continuity

Axiom A14 (Scale-coherence conservation):

$$\nabla_A T_R^{AB} = 0$$

In the weak-field flat-background continuum limit, the $B = 0$ component yields:

$$\partial_t \rho_R + \nabla \cdot \mathbf{J} + \partial_\sigma J^\sigma = 0$$

Burden can flow through space, flow along σ, and convert among internal channels, but it cannot appear or vanish without accounting.

39.3 Captured vs. Churn Split (Structural Refinement)

If the total burden is decomposed into captured and churn components $\rho_R = \rho_{\text{cap}} + \rho_{\text{churn}}$, introduce a conversion term Γ (capture/decay rate):

$$\partial_t \rho_{\text{cap}} + \nabla \cdot \mathbf{J}_{\text{cap}} + \partial_\sigma J^\sigma_{\text{cap}} = +\Gamma$$

$$\partial_t \rho_{\text{churn}} + \nabla \cdot \mathbf{J}_{\text{churn}} + \partial_\sigma J^\sigma_{\text{churn}} = -\Gamma$$

The constitutive form of Γ is completion-layer work.

40 GRAVITY AS SCALE-UPSHIFT: WEAK-FIELD SKELETON

This section implements Part 1's claim that gravity emerges when the sampler carries persistent captured structure that is costly to maintain, producing a scale-upshift that slows the local clock and reshapes local geometry. The geometric field is sourced by the full bipolar reconstruction burden.

40.0 Burden Density and Enclosed Mass Notation

The bipolar reconstruction cycle produces two local render burden densities at each spacetime point:

$$b_{q_+}(x), \quad b_{q_-}(x)$$

These are the pointwise densities of captured (persistent, coherent) structure maintained in each sector. The total local burden density sourcing geometry is:

$$b_{\text{tot}}(x) \;:=\; b_{q_+}(x) + b_{q_-}(x) \;\equiv\; \rho_{\text{cap}}(x)$$

Throughout §§40–44, ρ_{cap} and b_{tot} are the same object: the local density of captured render burden from both sectors. Gravity is sector-blind; it responds to b_{tot}, not to either sector individually.

For astrophysical applications (§44), the enclosed sector masses within radius r are:

$$M_{q_\pm}(r) \;:=\; \int_{|x'|\le r} b_{q_\pm}(x')\, d^3x', \qquad M_{\text{tot}}(r) = M_{q_+}(r) + M_{q_-}(r)$$

In the Poisson equations of §§37.5 and 40.1, $b_{\text{tot}}(x)$ is the source density. In the rotation-curve formulas of §44.4, $M_{q_\pm}(r)$ are the integrated enclosed masses. These are related by radial integration, not interchangeable.

40.1 Minimal Scale-Upshift Action

We adopt signature $(+,-,-,-)$ throughout, so $\Box = \partial_t^2 - \nabla^2$. Let $s_{\text{geom}}(x)$ represent the full-cycle geometric scale-upshift. A minimal action is:

$$S[s_{\text{geom}}] = \int d^4x \left(\frac{1}{2\kappa_s} (\partial_\mu s_{\text{geom}})(\partial^\mu s_{\text{geom}}) + s_{\text{geom}}\; b_{\text{tot}} \right)$$

Variation gives:

$$\Box\, s_{\text{geom}} = \kappa_s\, b_{\text{tot}}$$

In a static weak field:

$$\nabla^2 s_{\text{geom}} = -\,\kappa_s\, b_{\text{tot}}$$

Here $b_{\text{tot}}(x) = b_{q_+}(x) + b_{q_-}(x) \equiv \rho_{\text{cap}}(x)$ (§40.0) includes contributions from both sectors, gravity is sector-blind.

40.2 Newtonian Matching as Calibration

Define the Newtonian potential with the sign convention $\Phi_N < 0$ in an attractive well:

$$\Phi_N := -\,c_*^2\; s_{\text{obs}} = -\,\frac{c_*^2}{2}\; s_{\text{geom}}$$

Then from $\nabla^2 s_{\text{geom}} = -\,\kappa_s\, \rho_{\text{cap}}$:

$$\nabla^2 \Phi_N = \frac{c_*^2}{2}\; \kappa_s\; \rho_{\text{cap}}$$

Calibration hypothesis H4 (Newtonian regime): Match the right-hand side to $4\pi G \rho_{\text{mass}}$ in the appropriate regime. This fixes the mapping between render burden density and mass density (and fixes κ_s).

40.3 Weak-Field Vacuum Solution

In the static vacuum exterior of a spherically symmetric mass, $\rho_{\text{cap}} = 0$ and the field equation reduces to the Laplace equation:

$$\nabla^2 s_{\text{geom}} = 0$$

The spherically symmetric solution vanishing at infinity is:

$$s_{\text{geom}}(r) = \frac{B}{r}$$

for some constant $B > 0$ (positive because s_{geom} represents scale-upshift toward the mass).

Calibration. Matching to the Newtonian potential via $\Phi_N = -\,c_*^2\, s_{\text{obs}} = -\,c_*^2\, s_{\text{geom}}/2$ and requiring $\Phi_N = -\,GM/r$ gives:

$$s_{\text{geom}}(r) = \frac{2GM}{c_*^2\, r}$$

This is the weak-field geometric depth: valid for $s_{\text{geom}} \ll 1$, i.e., $r \gg 2GM/c_*^2$.

40.4 Time Dilation: Weak-Field Matching

The metric convention $g_{00} = e^{-s_{\text{geom}}}$ and the clock law $d\tau/d\tau_0 = \sqrt{g_{00}} = e^{-s_{\text{geom}}/2}$ (from the sector-clock theorem C7) give, in the weak-field regime:

$$\frac{d\tau}{d\tau_0} = e^{-s_{\text{geom}}/2} \approx 1 - \frac{s_{\text{geom}}}{2} = 1 - \frac{GM}{c_*^2\, r} = 1 + \frac{\Phi_N}{c_*^2}$$

This matches the standard GR weak-field time-dilation result $d\tau/dt \approx 1 + \Phi/c^2$.

Similarly, the weak-field metric component is:

$$g_{00} = e^{-s_{\text{geom}}} \approx 1 - s_{\text{geom}} = 1 - \frac{2GM}{c_*^2\, r}$$

which matches the linearised Schwarzschild form.

Since $\Phi_N < 0$, $d\tau < d\tau_0$: the local clock runs slower than the undilated clock at the same render index, as expected.

The agreement with the standard GR coefficient is a conditional consequence of the symmetric bipolar architecture (Conditional Result C7, §37.5): the geometric field is sourced by the full bipolar reconstruction cycle, producing s_{geom}, while the observable clock registers only the q_+-projected half-cycle through $d\tau/d\tau_0 = \sqrt{g_{00}} = e^{-s_{\text{geom}}/2}$. Given bipolar equipartition, station-

ary burden symmetry, and the observer source law with shared linearised coupling, this produces the correct GR coefficient.

40.5 Strong-Field Regime (Status)

The exact Schwarzschild metric

$$g_{00} = 1 - 2GM/(c_*^2 r)$$

corresponds to $s_{\text{geom}}(r) = -\ln(1 - 2GM/(c_*^2 r))$, which does not satisfy the linear Laplace equation $\nabla^2 s_{\text{geom}} = 0$. The minimal scalar action of §40.1 is a weak-field skeleton only; recovering the exact Schwarzschild solution requires a nonlinear generalization of the geometric field equation, either a self-interacting scalar field or a full metric-level construction.

This is completion-layer work. The weak-field skeleton correctly reproduces the linearised Schwarzschild regime, including the correct time-dilation coefficient. The strong-field regime (readout horizons, compact-object structure, exact vacuum solutions) requires extending §40.1 beyond the linear scalar approximation.

Connection to OSR (qualitative). A scale-upshift $s_{\text{geom}} > 0$ shifts the effective render index to $\sigma_{\text{eff}} = \sigma + s_{\text{geom}}$, increasing local OSR via $\text{OSR}(\sigma_{\text{eff}}) \propto e^{2\sigma_{\text{eff}}}$. This confirms that gravitational wells are sites of enhanced classicality (higher OSR = more stable reconstruction). However, the quantitative clock law is derived from the metric convention and the sector-clock theorem, not from raw OSR ratios.

40.6 Lens-Depth Parameter (Formal Definition)

Part 1 §16.4 classifies compact objects by how deep a synthesis band can imprint into accessible readout. The formal lens-depth parameter is:

$$\mathscr{L} := \frac{s_{\text{geom}}}{s_{\text{crit}}}$$

where s_{crit} is the critical geometric depth at which the outside observer's reconstruction can no longer maintain stable access to interior dynamics (the readout-horizon threshold). The L1–L5 taxonomy corresponds to increasing $\mathscr{L}$, from near-threshold coupling (L1, neutrino lens) to $\mathscr{L} \to 1$ (L5, readout horizon / black hole). Determining s_{crit} quantitatively requires the nonlinear strong-field generalization of the geometric field equation (§40.5) and is completion-layer work.

41 DRAG AND FLOW REGIMES AS OSR-DEPENDENT CLOSURE

Part 1 treats laminar vs. turbulent behavior as OSR-regime behavior of coherence transport. The mathematical place where that becomes actionable is the constitutive closure connecting ρ_R to its currents and stresses.

Write the spatial current as:

$$\mathbf{J} = \rho_R \, \mathbf{v} - \mathscr{D}(\sigma) \, \nabla \rho_R$$

Then continuity becomes:

$$\partial_t \, \rho_R + \nabla \cdot (\rho_R \, \mathbf{v}) = \nabla \cdot \left(\mathscr{D}(\sigma) \, \nabla \rho_R \right) - \partial_\sigma J^\sigma$$

A sampling-motivated scaling consistent with Part 1's "OSR is the viscosity dial" is:

$$\mathscr{D}(\sigma) \sim \frac{\ell_0^2}{\Delta t_*} \, \frac{1}{\mathrm{OSR}(\sigma)}$$

High OSR suppresses diffusion/noise (laminar, classical readout); low OSR amplifies it (turbulent, quantum-heavy readout).

The full derivation of $\mathscr{D}(\sigma)$ (and the full stress closure Π^{ij}, including pressure/shear decomposition) from alias statistics and closure algebra is completion-layer work.

42 HYDROGEN RING CALIBRATION: A, OSR, AND THE BOHR RADIUS

42.1 Hydrogen OSR Identification

Calibration hypothesis H5 (Hydrogen OSR):

$$\mathrm{OSR}_H \sim 1/\alpha \approx 137$$

Interpreting residual drift as the surviving fraction of null transport, the fine-structure constant measures how much non-phase-locked drift remains at the first fully stable atomic scale-ring. The fractional alias residue at the hydrogen band is α; the oversampling safety factor is $1/\alpha$.

42.2 Bohr Radius as OSR Inflation of a Base Length

Let the electron base length be identified with the reduced Compton wavelength $\bar{\lambda}_e = \hbar/(m_e c)$. Then OSR inflation yields the hydrogen length scale:

$$a_0 = \frac{1}{\alpha}\,\bar{\lambda}_e = \frac{\hbar}{m_e\, c\, \alpha}$$

The Bohr radius is the Compton length inflated by the oversampling safety factor.

43 REDSHIFT AS METRIC MISMATCH

43.1 Gravitational Redshift from the Clock Law

Gravitational redshift and gravitational time dilation are the same effect for stationary observers. A photon emitted at location A with geometric depth $s^{(A)}_{\text{geom}}$ and received at location B with geometric depth $s^{(B)}_{\text{geom}}$ undergoes a frequency shift:

$$\frac{\nu_B}{\nu_A} = \frac{d\tau_A}{d\tau_B} = \frac{e^{-s^{(A)}_{\text{obs}}}}{e^{-s^{(B)}_{\text{obs}}}} = e^{s^{(B)}_{\text{obs}} - s^{(A)}_{\text{obs}}}$$

In the Schwarzschild case, using $g_{00} = e^{-s_{\text{geom}}}$:

$$\frac{\nu_B}{\nu_A} = \sqrt{\frac{g^{(A)}_{00}}{g^{(B)}_{00}}}$$

which is the standard GR gravitational-redshift formula. The redshift law is not an OSR ratio; it follows from the same metric convention and sector-clock law that governs proper time (§§35.3, 40.3).

Connection to OSR (qualitative only). A scale-upshift that increases s_{geom} also increases the local OSR, shifting the system toward more classical behavior. OSR changes therefore accompany redshift, but the observable frequency shift is determined by the metric, not by taking OSR ratios directly.

43.2 Cosmic Redshift as Epoch Mismatch

A photon emitted in one epoch and received in another carries the imprint of the earlier sampler state. If the bridge constant $c_*(\sigma)$ has drifted between emission and reception, the photon's encoded frequency no longer matches the receiver's current reconstruction parameters. In the minimal picture, this is represented through epoch-dependent metric mismatch, with bridge-constant drift as the proposed underlying mechanism. The quantitative cosmological implementation, specifying which dimensionless ratios drift with $c_*(\sigma)$, is completion-layer work.

43.3 Unification of Redshift Types

All three redshift types are instances of the same structural phenomenon: emission encoded under one effective metric, reception decoded under another.

Gravitational redshift: different s_{geom} at emitter and receiver, same epoch. Cosmic redshift: different $c_*(\sigma)$ at emitter and receiver epochs. Accelerative redshift: different effective s_{geom} due to kinematic overhead.

The metric/clock law of §§35.3 and 40.3 governs all three quantitatively. OSR is the stability structure that accompanies these shifts, not the formula that computes them.

This section implements Part 1 §6.5's two-layer decomposition of dark-matter phenomenology: a universal hidden co-burden from the full bipolar cycle, and a scale-dependent enhancement from scale-clock running.

44.1 Hidden Co-Burden from the Full Bipolar Cycle

By the geometric source law (C7-i, §37.5), the geometric field is sourced by the total local burden density:

$$b_{\text{tot}}(x) = b_{q_+}(x) + b_{q_-}(x)$$

The visible sector accounts for b_{q_+} only. By bipolar equipartition (A13) and stationary burden symmetry (P6), $b_{q_-}(x) = b_{q_+}(x)$ for stationary symmetric configurations, so the total geometric source density is exactly twice the visible burden density at every point. (Real astrophysical systems are not perfectly stationary; small departures from exact sector symmetry are expected but do not affect the leading-order structure.) The hidden co-burden b_{q_-} is gravitationally active but not directly read out in q_+ electromagnetic observation.

44.2 Scale-Clock Enhancement

The scale-clock enhancement factor Ξ_σ captures the dependence of effective gravitational response on the system coordination index σ_{sys}, the global render index of the system as a collective structure:

$$G_{\text{eff}}(\sigma_{\text{sys}}) = G_0 \, \frac{\text{OSR}(\sigma_{\text{sys}})}{\text{OSR}(\sigma_{\text{ref}})} \;=:\; G_0 \, \Xi_\sigma$$

where σ_{ref} is the calibration render index (solar-system scale). At $\sigma_{\text{sys}} = \sigma_{\text{ref}}$, $\Xi_\sigma = 1$; at galactic σ_{sys}, $\Xi_\sigma > 1$.

Important distinction (cf. Part 1 §6.5). The system coordination index σ_{sys} and the local stability margin $\text{OSR}_{\text{local}}(r)$ at a specific position within the system are different variables. A galaxy has high σ_{sys} (driving $\Xi_\sigma > 1$) but can have low $\text{OSR}_{\text{local}}$ in its outskirts (producing nonlinear ren-

der response near the stability edge). The enhanced dark-matter effect in galaxy outskirts arises from the combination of both.

44.3 Combined Effective Gravitational Response

The total inferred mass from dynamics or lensing is:

$$M_{\text{eff}} = (M_{q_+} + M_{q_-})\, \Xi_\sigma$$

If $M_{q_-} = M_{q_+}$ (stationary burden symmetry, P6):

$$M_{\text{eff}} \approx 2\, M_{q_+}\, \Xi_\sigma$$

This separates the universal baseline (factor of ~ 2 from the full cycle) from the variable enhancement (Ξ_σ from scale-clock running).

44.4 Rotation Curves as the Structural Target

The rotation-curve formula requires specifying how the effective gravitational response varies with galactocentric radius r. Using the enclosed sector masses $M_{q_\pm}(r) = \int_{|x'|\le r} b_{q_\pm}(x')\, d^3x'$ (§40.0):

$$v^2(r) = \frac{G_{\text{eff}}\, (M_{q_+}(r) + M_{q_-}(r))}{r}$$

Here G_{eff} is determined by the system coordination index σ_{sys} of the galaxy as a whole (§44.2), which sets the scale-clock enhancement Ξ_σ. It is not a function of local position r in this minimal form. The position-dependent profile $v(r)$ arises from the enclosed mass profile $M(r)$, not from a varying $G_{\text{eff}}(r)$.

A more refined model could introduce a composite effective index that interpolates between the system-level σ_{sys} and the local stability margin $\text{OSR}_{\text{local}}(r)$ to capture outskirt nonlinearities. Such a composite model is the target needed to formally implement Part 1 §6.5's prediction that the strongest dark-matter excess appears in low-$\text{OSR}_{\text{local}}$ outskirts of high-σ_{sys} systems. Specifying this interpolation, the symmetry of the bipolar cycle (whether $M_{q_-} \approx M_{q_+}$ holds exactly or approximately), and the resulting $v(r)$ profile are completion-layer work. The minimal rotation-curve form presented here uses the global σ_{sys} only.

45 COMPLETION LAYER BOUNDARY

Part 2 stops exactly where Part 1's conceptual commitments stop being sufficient to fix a unique quantitative model. The following are explicitly deferred:

Slowdown law generalization: Extension of the minimal $e^{-2\sigma}$ form into full coherence-boundary scaling, including any exponent constraints and system-specific coordination costs.

Constitutive closures: Microderivation of $\mathscr{D}(\sigma)$, viscosity $\eta(\sigma)$, and capture/decay rate Γ from alias statistics and closure algebra.

The particle program: Mapping the 8-direction closure + bipolar cycle + winding modes to observed particle families, masses, and mixing angles.

Cosmology: Specifying which dimensionless ratios drift with $c_*(\sigma)$ and confronting CMB, BAO, and SNe datasets.

Strong field: The weak-field skeleton of §40 reproduces linearised Schwarzschild. Recovering the exact Schwarzschild metric requires a nonlinear generalization of the geometric field equation, either a self-interacting scalar field or a full metric-level construction. Quantitative read-out-horizon criterion and compact-object predictions (L1–L5 lens-depth taxonomy) depend on this extension.

Cross-sector coupling: Explicit suppression mechanism for q_--sector EM visibility and any residual cross-sector signatures.

Higher KK harmonics: Massive mode spectrum from the compact scale-phase coordinate beyond zero-mode truncation.

Hydrogen OSR derivation: Demonstrating that $\mathrm{OSR}_H = 1/\alpha$ follows from sampler microstructure rather than being adopted as a calibration hypothesis.

Sector-clock derivation from first principles: The factor-of-two is now conditionally derived (C7, §37.5) from bipolar equipartition (A13), stationary burden symmetry (P6), the observer source law (C7-ii), and shared linearised coupling (C7-iii). What remains is to derive these assumptions from the existing axioms (A1–A12): (a) prove that stable bipolar operation forces $\dim(P_{q_+}\mathscr{R}) = \dim(P_{q_-}\mathscr{R})$ without assuming it, likely via a variational principle or explicit exchange symmetry; (b) show that stationary configurations must have equal sector burdens, possibly via an exchange symmetry operator S with $SP_{q_+}S^{-1} = P_{q_-}$; (c) derive the observer source law, that s_{obs} responds to B_{q_+} through the same operator and coupling as s_{geom} responds to B_{tot}, from the sector-projector algebra; (d) formalise the 8-dimensional real closure space as an octonion algebra and exhibit the natural split into two 4-dimensional polar subspaces, providing the exchange symmetry automatically.

Bipolar symmetry quantification: Determining whether $M_{q_-} \approx M_{q_+}$ holds exactly (by architectural symmetry) or only approximately, and deriving the precise hidden co-burden fraction from the projector algebra and closure constraints.

46 GLOSSARY OF PART 2 FORMAL OBJECTS

46.1 Axioms

A1 (Carrier). A complex amplitude $F(\rho, \phi; \lambda) \in \mathbb{C}$ on the punctured scale plane $\Sigma = \mathbb{R}^2 \backslash \{0\}$, evolving in the ordering parameter λ. §28.1.

A2 (Bipolar drive). Rotating bipolar boundary condition at the puncture with factored form $F \to A(\rho) \sum_m h_m e^{im(\phi - \Omega\lambda)}$, $h_0 = 0$, first harmonic present and dominant. Shape coefficients h_m architecturally fixed; radial envelope $A(\rho)$ constrained by A3. §28.2.

A3 (Constant area throughput). The outward flux through any closed curve encircling the origin is constant: $\oint \mathbf{J} \cdot \hat{n}\, d\ell = \varsigma \cdot \Omega$. §29.1.

A4 (Finite representability). There exists a critical cumulative burden C_{crit} beyond which continuous pointwise readout becomes ill-posed. §31.1.

A5 (Ignition trigger). MSS ignition occurs at the critical radius ρ_0 where $C_H(\rho_0) = C_{\text{crit}}$. §31.2.

A6 (Discrete ticks). Post-MSS evolution is indexed by $n \in \mathbb{Z}$. §32.1.

A7 (Filterless binning). No anti-alias prefilter; stored bins are alias sums over the full reciprocal cell. §32.3.

A8 (Fourier readout). Each tick's readout is inverse Fourier synthesis from stored bins on the Brillouin zone $\mathscr{B}$. §32.4.

A9 (Unitary update). Stored bins evolve by a unitary multiplier $U_k = e^{-i\omega(k)\Delta t_*}$ each tick. §34.1.

A10 (Quadratic evolution). Massive modes acquire quadratic dispersion $\omega(k) = \omega_0 + c_* k^2/(2\mu)$ for $|k|\ell_0 \ll 1$. §35.1.

A11 (Closure cap). Each cell carries an internal bookkeeping state with eight independent directions; closure space $\mathscr{R}$, $\dim(\mathscr{R}) = 8$. §37.1.

A12 (Bipolar operator splitting). Full reconstruction cycle per tick: $\Psi_{n+1} = U_{q_-} U_{q_+} \Psi_n$ with orthogonal sector projectors. §37.2.

A13 (Bipolar equipartition). Equal closure capacity: $\dim(P_{q_+}\mathscr{R}) = \dim(P_{q_-}\mathscr{R}) = 4$. Architectural precondition for sector symmetry. §37.3.

A14 (Scale-coherence conservation). Continuity equation $\partial_t \rho_R + \nabla \cdot \mathbf{J} + \partial_\sigma J^\sigma = 0$ on $3 + 1 + \sigma$. §39.2.

46.2 Postulates

P6 (Stationary burden symmetry, local form). For stationary symmetric configurations: $b_{q_+}(x) = b_{q_-}(x)$ pointwise. §37.4.

46.3 Calibration Hypotheses

H1 (Mass scale). Mass parameter μ identified with $m_e c_* / \hbar_{\text{eff}}$ in a chosen slice. §35.2.

H2 (Planck-constant verification). Emergent $\hbar_{\text{eff}}$ from lattice Fourier uncertainty identified with measured $\hbar$; consistency check, not free parameter. §35.2.

H3 (Elementary charge). Unit charge fixed by matching e. §38.3.

H4 (Newtonian regime). Coupling κ_s fixed by matching $4\pi G \rho_{\text{mass}}$ in weak-field static limit. §40.3.

H5 (Hydrogen OSR). $\text{OSR}_H \sim 1/\alpha$ at the hydrogen scale-ring. §42.1.

46.4 Derived Results and Theorems

D1 (Radial slowdown). $J_\rho(\rho) = \varsigma \Omega / (2\pi\rho)$. From A3. §29.2.

D2 (Ignition scale, zero-core limit). $\rho_0 = \sqrt{\varsigma C_{\text{crit}} / (\pi \chi_H)}$. From T1 + A5. §31.2.

D3 (Non-injectivity). The readout map is not injective in a filterless sampler; the formal origin of quantum indeterminacy. §33.1.

D4 (Continuum-limit dispersion). $\omega(k) \approx c_* |k|$ for $|k| \ell_0 \ll 1$; massless photon-like transport. §34.2.

D5 (Bounded group velocity). $|v_g| \leq c_*$; maximal null-transport speed. §34.2.

D6 (Quantized charge labels). Integer winding numbers from the compact phase fiber; positive and negative charges from opposite winding orientations. §38.3.

T1 (Unavoidable ramp). $C_H(\rho) \propto \chi_H \, \rho^2 \to \infty$. Under A1–A3, cumulative spectral burden grows without bound. §30.2.

C7 (Sector-clock factor). $s_{\text{geom}} = 2\, s_{\text{obs}}$ in the linearised symmetric bipolar regime. Requires A13 (architectural), P6 (local form), C7-ii (observer source law), C7-iii (shared coupling/ boundary conditions). §37.5.

C7-i (Geometric source law). $\nabla^2 s_{\text{geom}} = -\,\kappa_s\, b_{\text{tot}}$. §37.5.

C7-ii (Observer source law). $\nabla^2 s_{\text{obs}} = -\,\kappa_s\, b_{q_+}$. Separate postulate; not derived from A13 or P6. §37.5.

C7-iii (Shared coupling and boundary conditions). Same κ_s and vanishing-at-infinity conditions for both depth fields. §37.5.

46.5 Key Formal Objects

$A(\rho)$ **(Radial envelope).** Radial amplitude factor in A2; constrained by A3, not independently free. §28.2.

$\mathscr{B}$ **(Brillouin zone).** First Brillouin zone of the lattice Λ; the representable momentum band. §32.3.

$b_{q_\pm}(x)$ **(Local sector burden densities).** Pointwise render burden density per sector: $b_{q_\pm}(x) = \langle \Psi(x) \,|\, P_{q_\pm} \,|\, \Psi(x) \rangle_{\text{render}}$. §37.4, §40.0.

$b_{\text{tot}}(x)$ **(Total local burden density).** $b_{\text{tot}} = b_{q_+} + b_{q_-} \equiv \rho_{\text{cap}}$. Sources the geometric Poisson equation. §40.0.

c_* **(Null-transport speed).** $c_* = \ell_0 / \Delta t_*$. Maximal phase-transport speed on the lattice; the emergent speed of light. §27.4, §34.2.

$C_H(\rho)$ **(Cumulative spectral burden).** $C_H = \pi \chi_H \rho^2 / \varsigma$ (zero-core limit). Monotone crowding variable triggering ignition at C_{crit}. §30.1.

C_{crit} **(Representability threshold).** Critical burden beyond which continuous readout fails. §31.1.

χ_H **(Source-shape factor).** $\chi_H = \sum_{m\neq 0} m^2 \,|\, h_m \,|^2 \,/ \sum_{|m|=1} \,|\, h_m \,|^2$. Equals 1 for any pure first-harmonic source; > 1 for higher-harmonic profiles. Architecturally fixed. §28.2.

Δt_* **(Tick period).** Fundamental MSS period. §27.4.

ϵ **(Finite-core regularization radius).** Inner cutoff in the cumulative burden integral; formal derivations adopt $\epsilon \to 0$. §28.2, §30.1.

$g(\phi;\lambda)$ **(Regularized pre-limit trace).** $g(\phi;\lambda) = \lim_{\rho\to\rho_0^-} F(\rho,\phi;\lambda)$. MSS's sole causal input; existence assumed as regularity postulate. §31.4, §31.6.

g_{00} **(Metric temporal component).** $g_{00} = e^{-s_{\text{geom}}}$; the convention linking geometric depth to emergent 4D metric. §35.3, §40.2.

$G_{\text{eff}}(\sigma_{\text{sys}})$ **(Effective gravitational constant).** $G_{\text{eff}} = G_0\,\Xi_\sigma$; enhanced at high system coordination index. §44.2.

h_m **(Shape coefficients).** Dimensionless, architecturally fixed angular Fourier coefficients of the bipolar source; $h_0 = 0$, $\sum_{|m|=1} |h_m|^2 > 0$. §28.2.

κ_s **(Burden-geometry coupling).** Coupling constant in the geometric Poisson equation $\nabla^2 s_{\text{geom}} = -\kappa_s\, b_{\text{tot}}$. Fixed by H4. §40.1, §40.3.

Λ **(Reconstructed lattice).** $\Lambda = \ell_0\,\mathbb{Z}^3$. The discrete spatial grid on which readout fields are defined. §32.1.

ℓ_0 **(Lattice spacing).** Fundamental cell length. §27.4.

$\mathscr{L}$ **(Lens-depth parameter).** $\mathscr{L} = s_{\text{geom}}/s_{\text{crit}}$. Classifies compact objects from L1 (near-threshold) to L5 (readout horizon). §40.6.

$M_{q_\pm}(r)$ **(Enclosed sector masses).** $M_{q_\pm}(r) = \int_{|x'|\le r} b_{q_\pm}(x')\,d^3x'$. Radial integrals of local burden densities; enter rotation-curve formulas. §40.0, §44.4.

$P_{q_\pm}$ **(Sector projectors).** Orthogonal projectors on $\mathscr{R}$: $P_{q_+} + P_{q_-} = I$, $P_{q_+}P_{q_-} = 0$. Define visible and hidden sectors. §37.2.

$\Psi_n(x)$ **(Operational field).** $\Psi_n : \Lambda \to \mathscr{R}\otimes\mathbb{C} \cong \mathbb{C}^8$. Sector-valued reconstruction state at tick n. §32.1, §37.1.

$\mathscr{R}$ **(Closure space).** 8-dimensional real vector space ($\dim(\mathscr{R}) = 8$), consistent with octonionic algebra. Carries sector projectors and closure constraints. §37.1.

ρ_0 **(Ignition radius).** Critical radius where $C_H = C_{\text{crit}}$; MSS ignition locus. §31.2.

ρ_R **(Render burden density).** T_R^{00} component of the render stress tensor; total local burden including both captured and churn contributions. §39.1.

$s_{\text{geom}}(x)$ **(Geometric depth).** Full-cycle scale-upshift field sourcing emergent geometry. Satisfies $\nabla^2 s_{\text{geom}} = -\kappa_s\, b_{\text{tot}}$ in weak-field static limit. §40.1.

$s_{\text{obs}}(x)$ **(Observer depth).** q_+-projected depth governing proper time: $d\tau/d\tau_0 = e^{-s_{\text{obs}}}$. In the linearised symmetric bipolar regime, $s_{\text{obs}} = s_{\text{geom}}/2$ (C7). §35.3.

T_R^{AB} **(Render stress tensor).** Symmetric tensor on $3 + 1 + \sigma$ encoding burden density, spatial flow, scale transport, and directional stresses. §39.1.

ς **(Pre-MSS constant).** Throughput-to-rotation ratio. Given the architecturally fixed source profile, ς is the single free parameter of the pre-MSS regime. §29.3.

Ξ_σ **(Scale-clock enhancement).** $\Xi_\sigma = \text{OSR}(\sigma_{\text{sys}})/\text{OSR}(\sigma_{\text{ref}})$. Near unity at solar-system scale; > 1 at galactic scale. §44.2.